PHILOSOPHICAL TRANSACTIONS OF THE ROYAL SOCIETY A MATHEMATICAL, PHYSICAL & ENGINEERING SCIENCES

On the Stability of Three-Dimensional Boundary Layers with Application to the Flow Due to a Rotating Disk

N. Gregory, J. T. Stuart and W. S. Walker

Phil. Trans. R. Soc. Lond. A 1955 **248**, 155-199
doi: 10.1098/rsta.1955.0013

ON THE STABILITY OF THREE-DIMENSIONAL BOUNDARY LAYERS WITH APPLICATION TO THE FLOW DUE TO A ROTATING DISK

By N. GREGORY, J. T. STUART and W. S. WALKER

Aerodynamics Division, National Physical Laboratory

(*Communicated by Sir Edward Bullard, F.R.S.—Received* 11 *January* 1955—*Read* 21 *April* 1955)

(Plates 1 and 2)

CONTENTS

A phenomenon of boundary-layer instability is discussed from the theoretical and experimental points of view. The china-clay evaporation technique shows streaks on the surface, denoting a vortex system generated in the region of flow upstream of transition. Experiments on a swept wing are described briefly, while experiments on the flow due to a rotating disk receive much greater attention. In the latter case, the axes of the disturbance vortices take the form of equi-angular spirals, bounded by radii of instability and of transition. A frequency analysis of the disturbances shows that there is a narrow band of disturbance components of high amplitude, some frequencies within this band corresponding to disturbances fixed relative to the surface and others corresponding to moving waves. Furthermore, the determination of velocity profiles for the rotating-disk flow is described, the agreement with the theoretical solution for laminar flow being quite satisfactory; for turbulent flow, however, the empirical theories are not very satisfactory.

In order to explain the vortex phenomenon just discussed, the general equations of motion in orthogonal curvilinear co-ordinates are examined by superimposing an infinitesimal disturbance periodic in space and time on the main flow, and linearizing for small disturbances.

An important result is that, within the range of certain approximations, the velocity component in the direction of propagation of the disturbance may be regarded as a two-dimensional flow for stability purposes; then the problem of stability formally resembles the well-known two-

VOL. 248. A. 943. (Price 17*s*. 6*d*.) 20 [Published 14 July 1955

dimensional problem. However, it is important to emphasize that this result—namely, that the flow curvature has little influence on stability—is applicable only to the possible modes of instability in a local region. The nature of three-dimensional flows is discussed, and the importance of co-ordinates along and normal to the stream-lines outside the boundary layer is examined. In accord with the formal two-dimensional nature of the instability, there is a whole class of velocity distributions, corresponding to different directions, which may exhibit instability.

The question of stability at infinite Reynolds number is examined in detail for these profiles. As for ordinary two-dimensional flows, the wave velocity of the disturbance must lie somewhere between the maximum and minimum of the velocity profile considered. The points where the wave velocity equals the fluid velocity are called critical points, of which most of the profiles considered have two. Then Tollmien's criterion that velocity profiles with a point of inflexion are unstable at infinite Reynolds number is extended to the case of profiles with two critical points. One particular profile—namely, that for which the point of inflexion lies at the point of zero velocity—may generate neutral disturbances of zero phase velocity, corresponding to the disturbances visualized by the china-clay technique. A variational method for the solution of certain of the eigenvalue problems associated with stability at infinite Reynolds number is derived, found by comparison with an exact solution to be very accurate, and applied to the rotating disk. The fixed vortices predicted by the theory have as their axes equi-angular spirals of angle 103°, in good agreement with experiment, but the agreement between theoretical and experimental wave number is not good, the discrepancy being attributed to viscosity. Finally, the correlation between the experimentally observed and theoretically possible disturbances is discussed and certain conclusions drawn therefrom. The streamlines of the disturbed boundary layer show the existence of a double row of vortices, one row of which produces the streaks in the china clay. Application of the theory to other physical phenomena is described.

1. Introduction

The fundamental experimental researches of Osbourne Reynolds (1883), G. I. Taylor (1923), Schubauer & Skramstad (1943) and others have considerably stimulated the development of theories of hydrodynamic stability. Almost all the published work on the subject concerns two-dimensional or axi-symmetrical mean motions, and there has been little or no systematic research on the stability of three-dimensional fluid flows. The present paper describes some experimental and theoretical work on the latter subject, but before explaining the scope of this work it is convenient to classify previous work on hydrodynamic stability into three types, as follows:

(*a*) *Dynamic instability*

In this case the instability is produced by centrifugal force or an external field of force such as that due to gravity. An examination of the forces on a fluid particle shows that a viscous flow over a concave surface is dynamically unstable, while the flow over a convex surface is dynamically stable (Kármán 1934). An example of the unstable case occurs in the flow between two concentric cylinders when the inner one rotates and the outer is at rest. The disturbances take the form of steady, cellular vortices with periodicity along the axis of the cylinders, as demonstrated mathematically and experimentally by Taylor (1923). A similar phenomenon occurs in the boundary-layer flow over a concave surface (Görtler 1940; Liepmann 1945), the vortices having their axes in the direction of the mean flow.

(*b*) *Inflexional instability*

It has been known since the time of Lord Rayleigh (1880) that two-dimensional velocity distributions which contain a point of inflexion are unstable at infinite Reynolds number.

Tollmien (1935) has shown that, for flows in channels and in boundary layers, the presence of a point of inflexion is a necessary and sufficient condition for instability. Jets and wakes also exhibit this type of instability, as shown by the work of Hollingdale (1940), Savic (1941) and Pai (1951). A physical explanation in terms of momentum transfer was given by Taylor (1915), and Lin (1945) has related the instability to the nature of the vorticity field of the mean flow. The disturbances take the form of progressive waves, with periodicity in the direction of the mean flow. At finite Reynolds numbers the wave velocity and wave-length of the disturbance are modified by viscosity; its effect on a boundary-layer flow differs considerably from that on a jet or wake flow because of the presence of a wall.

(*c*) *Viscous instability*

Many two-dimensional velocity distributions are stable at infinite Reynolds number and are destabilized only by the action of viscosity, which makes possible the growth of the Reynolds shear stress necessary for the transfer of energy from the mean flow to the disturbance. The work of Heisenberg (1924), Tietjens (1925), Tollmien (1929), Schlichting (1933, 1935) and Lin (1945) has laid bare the fundamental processes of the instability, and the calculations of Tollmien and Schlichting have been amply confirmed by the experiments of Schubauer & Skramstad (1943). It appears that the disturbance is dominated by viscosity in two regions in the flow; one region is a secondary boundary layer adjacent to the wall, and the other is a viscous layer at the station where the velocity of the progressive wave disturbance equals the velocity of the fluid. This inner friction layer is related to a singularity in the solution of the Orr–Sommerfeld equation, which governs the mathematical problem. An additional result, due to Squire (1933), is that the flow is more stable for three-dimensional than for two-dimensional disturbances, so that it is necessary to consider only the latter. Thus the disturbances which appear physically are two-dimensional waves, as for inflexional instability.

Turning to previous work on the three-dimensional problem, we note that attempts at an estimation of the effects of three-dimensionality on the stability of boundary layers have been made by Jones (1947), Sears (1948) and Kuethe (1950), and that Shibuya (1951) has tackled the specific problem of the flow due to a rotating disk near to a fixed and parallel wall. Jones and Sears concluded that, since the steady flow in the boundary layer of a yawed infinite cylinder is independent of the spanwise distance, its stability is determined by the chordwise component of velocity only. The work described in this paper shows this conclusion to be fallacious. Moreover, Shibuya's work neglects the radial component of the flow due to the rotating disk, again in disagreement with the results of this paper. On the experimental side, fluctuations in the boundary layer of a rotating disk were noticed by Smith (1947) and by Theodorsen & Regier (1947), using a hot-wire technique, but no systematic research on these fluctuations appears to have been pursued until the work described in the present paper was initiated.

This work forms part of an intense basic investigation into the subject which has been pursued at the Royal Aircraft Establishment and at the National Physical Laboratory. It arose from flight tests on aircraft with swept-back wings conducted at the R.A.E. by Gray, who perceived that the boundary layer of a swept wing became turbulent much closer

PHILOSOPHICAL TRANSACTIONS OF THE ROYAL SOCIETY A MATHEMATICAL, PHYSICAL & ENGINEERING SCIENCES

to the leading edge than on a corresponding unswept wing. Just upstream of transition, evaporation methods for indicating the state of the boundary-layer flow suggested the existence in the layer of stationary rows of regularly spaced vortices with axes lying in the streamwise direction. This phenomenon was confirmed by experiments on large swept wings in wind tunnels, both at the R.A.E. by Anscombe & Illingworth, and at the N.P.L. by Gregory & Walker, whose experiments are summarized in part I, § 3, while theoretical work by Squire, Owen & Randall and Stuart (see part II) revealed the essential mechanism of the instability by which the disturbance vortices are generated.

The main experimental work described in part I concerns the flow due to a rotating disk, which exhibits a similar type of instability to that of a swept-wing boundary layer. The reasons for investigating the three-dimensional boundary layer on a rotating disk rather than on, say, a swept wing, are as follows. First, there exists an exact solution of the Navier–Stokes equations for this particular study in compressible flow (Kármán 1921), and the velocity distribution of the laminar flow has been calculated by Cochran (1934). Moreover, the shape of the laminar velocity profiles and the thickness of the boundary layer are independent of the radius. The flow is thus much simpler to describe than that over a swept wing, where the displacement thickness and components of velocity vary along the streamlines because of the pressure gradients. It is, for example, easier to relate the critical Reynolds number of the instability to the velocity distribution if the *shape* of the latter is independent of position, as it is for the flow due to a rotating disk. It was felt that advantages such as these outweighed any drawbacks which might be associated with a moving surface. The measurements undertaken on the rotating disk comprise (i) the measurement of velocity distributions in the laminar, perturbed and turbulent regions of flow; (ii) the determination of criteria for instability of the laminar flow and transition to turbulence, and (iii) the determination of the nature of the disturbance produced. The fluctuations observed by Smith (1947) are roughly in agreement with the present investigation, but his paper does not show the physical nature of the instability.

In part II, the general equations of motion in orthogonal curvilinear co-ordinates are examined for periodic disturbances of an arbitrary geometrical configuration, and the corresponding equations which govern the hydrodynamic stability of three-dimensional boundary-layer flows are obtained. These equations include as particular cases the equations obtained in the past for special types of hydrodynamic stability. At a local station in the flow, the equations of stability, with certain approximations, are found to resemble formally those for two-dimensional flows; the relevant mean-flow velocity is the component in the direction of propagation of the disturbance at that particular station. This result greatly simplifies the analysis, and the remainder of the theory stems from this. It is found that in a three-dimensional boundary layer there can exist both progressive-wave and fixed-vortex types of disturbance, the former being geometrically analogous to Tollmien–Schlichting waves and the latter (in a lesser degree) to Taylor–Görtler vortices. The theory is applied to the case of the rotating-disk flow, and correlation is obtained between the theoretical form of the vortex pattern and the streaks on the surface which are revealed by the china-clay technique.

Finally, in § 17, other examples of the effects of a three-dimensional boundary-layer instability are discussed.

2. Notation

α, β, γ	orthogonal curvilinear co-ordinates (γ normal to surface)
$\mathrm{d}s$	element of length
h_ν $(\nu = 1, 2)$	given by $\mathrm{d}s^2 = h_1^2 \mathrm{d}\alpha^2 + h_2^2 \mathrm{d}\beta^2 + \mathrm{d}\gamma^2$
$\mathbf{v}$	velocity
$\boldsymbol{\omega}$	vorticity
p	pressure
ρ	density
ν	kinematic viscosity
μ	viscosity
t	time
$\mathbf{V} \equiv (U, V, W)$	main-flow velocity
$\boldsymbol{\Omega} \equiv (\xi_0, \eta_0, \zeta_0)$	main-flow vorticity
P	main-flow pressure
$\mathbf{v}_1'$	disturbance velocity
$\boldsymbol{\omega}_1'$	disturbance vorticity
p_1'	disturbance pressure
n	wave number of disturbance
λ	frequency of disturbance
$\mathbf{v}_1 \equiv (u, v, w)$	given by $\mathbf{v}_1' \equiv \mathbf{v}_1 \exp \mathrm{i}(n\alpha - \lambda t)$
$\boldsymbol{\omega}_1 \equiv (\xi_1, \eta_1, \zeta_1)$	given by $\boldsymbol{\omega}_1' \equiv \boldsymbol{\omega}_1 \exp \mathrm{i}(n\alpha - \lambda t)$
p_1	given by $p_1' \equiv p_1 \exp \mathrm{i}(n\alpha - \lambda t)$
Q	given by $\operatorname{div} \mathbf{v}_1' = Q \exp \mathrm{i}(n\alpha - \lambda t)$
x, y, z	dimensionless forms of α, β, γ; for use as fluid-motion co-ordinates (z normal to surface)
$\overline{U}, \overline{V}, \overline{W}$	dimensionless main-flow velocity
l	length scale of system
δ	length scale of boundary layer (and variational operator)
δ_1	displacement thickness
δ_2	momentum thickness
V_0	a characteristic speed (speed outside boundary layer or local speed of rotating disk)
p_2	$\delta p_1 / \mu$
σ	$n\delta / h_1$, dimensionless wave number
c	$\lambda h_1 / n V_0$, dimensionless phase velocity
R	$V_0 \delta / \nu$, Reynolds number
m_{12}	$(\delta / h_1 h_2)\, \partial h_1 / \partial \beta$
m_{21}	$(\delta / h_1 h_2)\, \partial h_2 / \partial \alpha$
m_{13}	$(\delta / h_1)\, \partial h_1 / \partial \gamma$
m_{23}	$(\delta / h_2)\, \partial h_2 / \partial \gamma$
δ_ν'	$\dfrac{1}{h_\nu} \dfrac{\delta}{l}$ $(\nu = 1, 2)$
δ_3'	δ / l

z_1, z_2	points where $\bar{U}=c$
z_δ	edge of boundary layer
$K(z)$	$-\dfrac{\mathrm{d}^2\bar{U}}{\mathrm{d}z^2}\Big/(\bar{U}-c)$
ω	angular velocity of rotating disk
r	radius
ϵ	angle between direction of propagation of disturbance and radius
r, ϕ, γ	cylindrical co-ordinates for rotating disk
v_r, v_ϕ, v_γ	velocity components for rotating disk
V_T	total velocity parallel to disk
$F, G \equiv (v_r, v_\phi)/\omega r$	non-dimensional velocities for rotating disk
τ_0	surface shear stress
$R_r = r^2\omega/\nu$	Reynolds number based on radius and local disk velocity
Φ	direction of resultant flow parallel to disk measured outwards from tangential direction
$\zeta \equiv \gamma\sqrt{(\omega/\nu)}$	for distance normal to disk
H	δ_1/δ_2

Part I. Experimental

By N. Gregory and W. S. Walker

3. Brief description of experiments on a swept wing

By way of introduction to the detailed experimental investigation of the instability on the rotating disk, this section summarizes the exploratory observations on the instability obtained at the National Physical Laboratory on a swept wing in the 13 × 9 ft. wind tunnel. The experiments were performed concurrently with those of Anscombe & Illingworth at the Royal Aircraft Establishment, and sought wind-tunnel confirmation of Gray's flight observations of forward transition.

Gray's empirical analysis of his observations suggested that critical conditions would be obtained in the 13 × 9 ft. wind tunnel where the maximum speed is limited to 210 ft./s only on an aerofoil with nose radius of curvature greater than 1 in. On a conventional section, such a radius is only found for a chord rather greater than that usually tested in this tunnel. The tests were therefore carried out on a 30 in. chord model of the 30 % Griffith suction aerofoil which had a nose radius of 1·35 in. This aerofoil had been previously tested by Richards, Walker & Taylor (1945) and Gregory & Walker (1946). Round fairings of balsa were fitted at each end of the 9 ft. span of the aerofoil, which was mounted horizontally in the tunnel at zero incidence as a finite aspect ratio wing (figure 1, plate 1). The pedestal support from the floor turn-table enabled the angle of yaw to be altered easily.

The wing was coated with china clay for visualization of the transition front. In this technique the china-clay coat is evenly sprayed with methyl salicylate which renders the china clay transparent. Evaporation of the liquid due to the boundary-layer flow proceeds more quickly where the boundary layer is turbulent than where it is laminar owing to the greater shearing stresses. After a time, the line of transition is usually depicted, the area of turbulent flow being dry, and the laminar flow being wet.

The pressure gradients over the mid-span section were found to be favourable to about 0·6 chord at all angles of sweep. Farther aft, between 0·73 and 0·77 chord, the flow separated as the boundary-layer control required at the aerofoil slots (0·8 chord) was not in use.

The effect of the angle of sweep on chordwise position of the transition front as visualized by the china-clay method is shown in figure 2. At sweep angles of 45° and above, a wind speed below the top speed of the tunnel was found, above which the transition position moved rapidly to the leading edge. With increasing sweep angle, the critical wind speed was lowered, and the range of speed through which the transition position moved to the leading edge was much reduced.

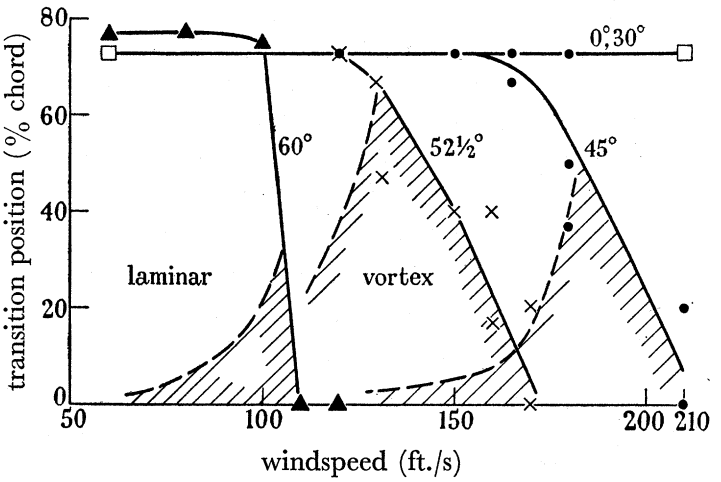

FIGURE 2. Variation of extent of laminar and vortex-flow regimes with wind speed and sweep angle on 2½ ft. chord 30 % Griffith aerofoil.

Under all conditions in which transition is affected, narrow, regular traces are observed in the china-clay picture, starting at the leading edge and running approximately parallel to the local flow, which is spanwise along the stagnation generator and curves rapidly round into the downstream direction. These traces appear to denote the presence of stationary vortices in the boundary layer, similar indications having previously been found by Gregory & Walker (1950) in the case of Görtler vortices which arise from the instability of a boundary layer on a concave surface, and in the case of flow round excrescences (figure 19, plate 2). With increasing speed, the vortices are observed right back to the transition front (figure 3, plate 1). In this figure, a long exposure to the wind was required and the china clay has dried out completely at the front owing to the thin boundary layer. The circular patches on the aerofoil are caused by plugs of Plasticine which absorb the methyl salicylate and should be disregarded, as should the two firm wedges of turbulent flow arising from excrescences on the aerofoil surface, and the turbulent state of the flow over the end fairings, on which vortex traces were also visible.

A wedge of turbulence was also produced by a large excrescence placed on the front stagnation line. When the angle of sweep and wind speed were raised to a value where transition is brought forward by reason of the instability, the turbulence appears to spread outwards along the swept leading edge and to contaminate the remainder of the wing. This confirms a phenomenon which has also been observed in flight by Gray.

These experiments amply substantiate the existence of a laminar-boundary-layer instability due to the three-dimensionality of the flow. In view of the more tractable conditions obtaining in the particular case of the three-dimensional flow due to a rotating disk, the experiments on the swept 30 % Griffith aerofoil were not taken further.

4. Apparatus and techniques for the rotating disk

The experiments were carried out on a 12 in. diameter solid disk which was cut from $\frac{1}{4}$ in. thick Perspex and mounted on a fractional horse-power d.c. motor. The outward-facing side of the disk was smooth and was coated with china clay for transition indication; the reverse side was painted black to increase the contrast. A variable resistance allowed any speed up to 3000 rev/min to be obtained, and the speed was ascertained stroboscopically.

The boundary-layer velocity profiles were measured with exploring tubes carried on a combined traversing and yawing mechanism, the displacements being indicated on Veeder counters which registered to thousandths of an inch in traverse and 0·2° in yaw. A total head tube was fashioned from nickel hypodermic tubing which had been flattened and ground so that the mouth was of rectangular form with walls 0·0025 in. thick and an aperture of 0·0015 in. The yawmeter head which was used on the solid disk was of the Conrad type with an included angle of 45° between the faces. The walls of this instrument were 0·0050 in. thick with an aperture of 0·0035 in. The yawmeter was calibrated in a wind tunnel by traversing through the boundary layer of a flat plate, which was assumed to be uni-directional.

In the experimental traverses, the yawmeter was used only for obtaining the direction of the local flow with a null reading, as the instrument was treated with some suspicion owing to its small size. The total head was obtained in a subsequent traverse with the total head tube alined in the directions indicated by the yawmeter traverse. The position of contact of the traversing tubes with the surface was obtained when the disk was rotating by listening for the first whisper of rubbing contact. Care had to be taken not to press the tubes firmly on to the surface as this scored the china clay and was liable to partly choke the mouth of the tubes and alter the calibration of the yawmeter. An additional uncertainty present with the use of a yawmeter in a total head gradient is that if the effective centres of the two tubes are not in a plane parallel to the surface, an erroneous indication of the flow direction may be given. In addition, the disk was not flat to within $\pm$0·002 in., and the tubes which were of total width 0·0075 and 0·0135 in. were large compared with the thickness of the boundary layer measured, which was of the order of 0·035 in. Owing to all these hazards, it is suggested that the uncertainty of the measurements may be of the order of $\pm$0·002 in. in distance and $\pm$4° in yaw.

5. Criteria for the onset of instability and transition

Preparatory to the measurement of velocity profiles, the transition position was found at a number of rotational speeds by the china-clay technique. A typical example of the pattern obtained from the disk is that shown in figure 4, plate 2. Two critical radii are indicated separating three regimes of flow. Within the inner radius the flow is purely laminar, and beyond the outer radius, wholly turbulent. In between, a series of traces in

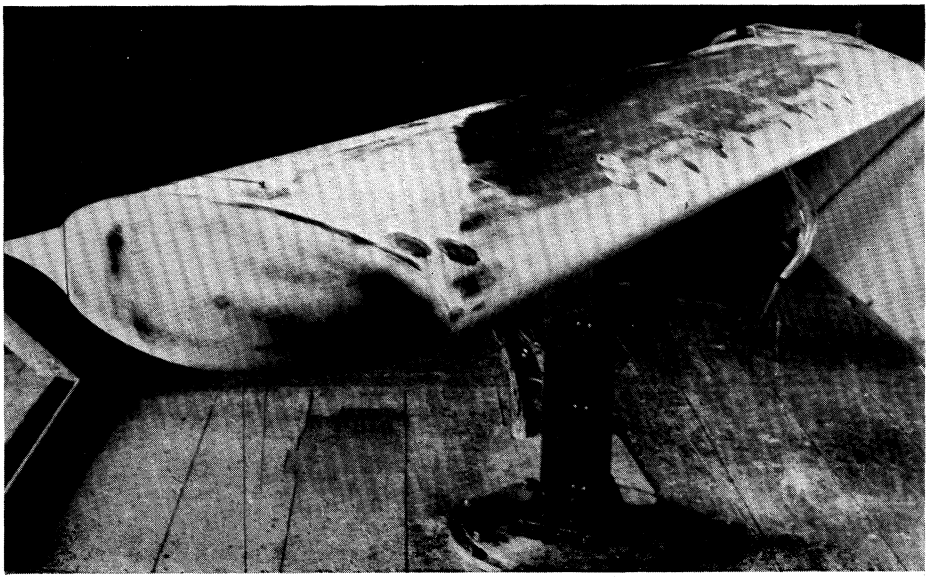

FIGURE 1. General view of arrangement of 30 % Griffith aerofoil in tunnel. Sweep angle 60°. Transition at 100 ft./s.

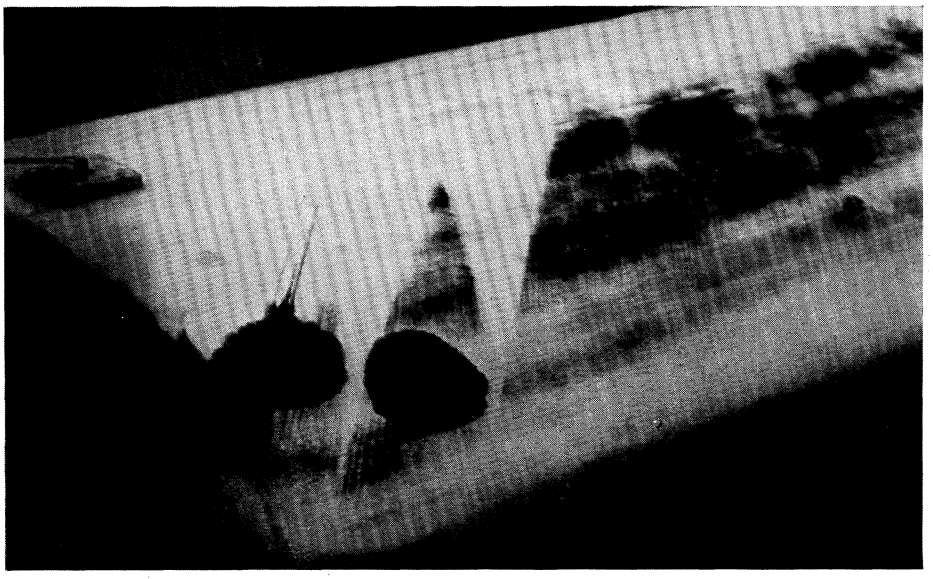

FIGURE 3. China-clay record of vortex traces persisting to transition at 0·4 chord on 30 % Griffith aerofoil. Sweep angle 45°. Wind speed 180 ft./s.

(*Facing p.* 162)

PHILOSOPHICAL TRANSACTIONS OF THE ROYAL SOCIETY A MATHEMATICAL, PHYSICAL & ENGINEERING SCIENCES

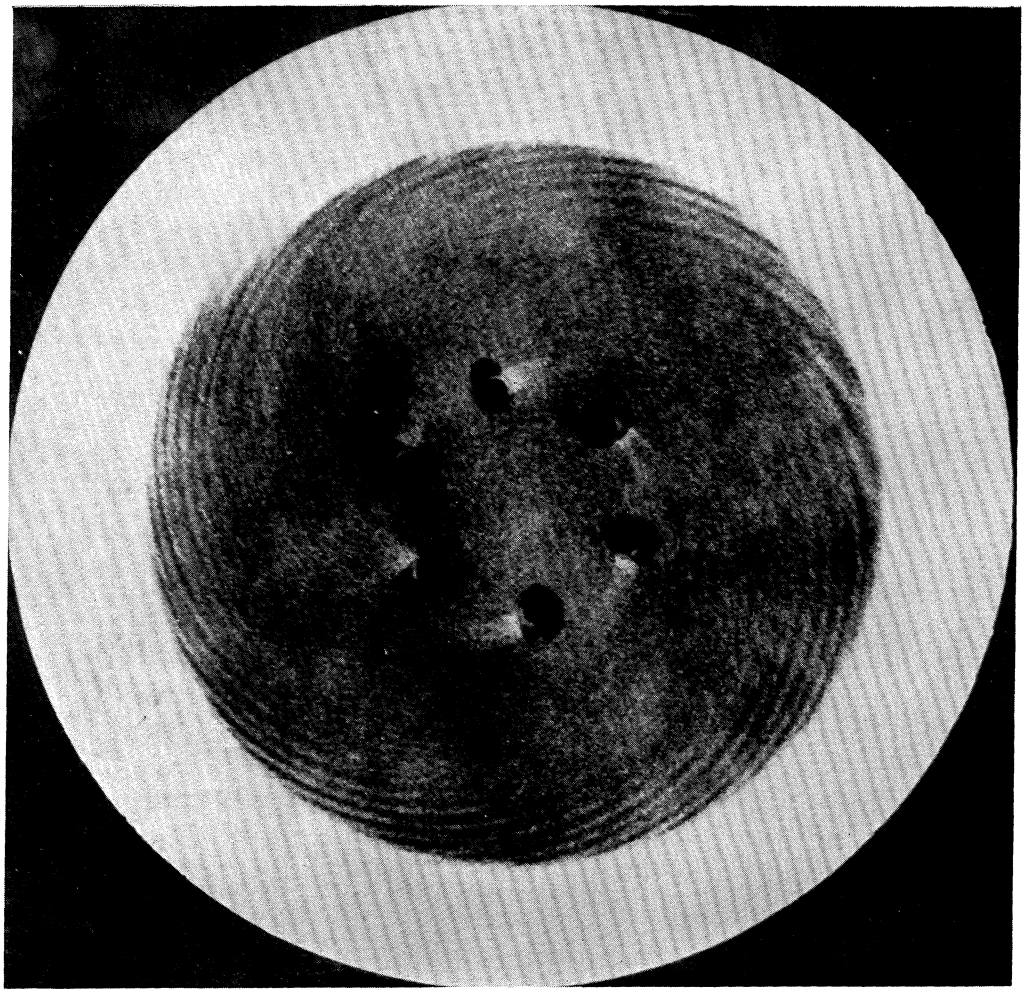

FIGURE 4. China-clay record of instability and transition on a rotating disk. Direction of rotation of disk: anti-clockwise. Rotational speed 3200 rev/min. Radius of disk 6 in. Radius at start of instability 3·5 in. R_r ($\equiv r^2\omega/\nu$) = 182000. Radius at transition 4·35 in. $R_r = 282000$.

FIGURE 19. China-clay record of vortex structure of a turbulent wake on a flat plate. Cylindrical excrescence, height 0·04 in., diameter 0·2 in. 0·75 ft. from leading edge; wind speed 40 ft./s.

PHILOSOPHICAL TRANSACTIONS OF THE ROYAL SOCIETY A MATHEMATICAL, PHYSICAL & ENGINEERING SCIENCES

the form of equi-angular spirals are recorded in the china clay. Such traces appear to indicate the presence of stationary vortices lying in the boundary layer, as in the case of the swept wing; a discussion on the full significance of these observations is given with the aid of additional evidence in § 7 below.

Use was also made of a simple form of acoustical stethoscope. By listening at one end of a short length of 0·25 in. bore plastic tubing, the other end of which was held in the boundary layer about 0·01 in. from the rotating surface, one could detect the critical radii as accurately as with the china clay, for there was silence in the laminar region, a note of fairly definite pitch in the middle region due to the rapid succession of vortices past the tube, and the typical turbulent roar in the turbulent region.

The measured Reynolds numbers ($r^2\omega/\nu$) at the start of the instability (vortex) region and at transition to turbulence are given in table 1. The values are practically constant, being independent of the speed of rotation. Turbulence in the surrounding fluid is probably responsible for the slight scatter, as it is significant that the highest value of Reynolds number at transition, 299 000, was obtained from the first observation that was made one Monday morning when the air in the room was at its stillest. This compares well with the value of 310 000 obtained by Smith (1947) with hot-wire apparatus on a more carefully made, polished steel disk.

TABLE 1. MEASUREMENTS OF THE ONSET OF INSTABILITY AND OF TRANSITION ON THE 1 FT. DIAMETER ROTATING DISK

	onset of instability		transition	
disk speed (rev/min)	radius (in.)	$10^{-5}R_r$	radius (in.)	$10^{-5}R_r$
3200	3·50	1·82	4·35	2·82
2900	3·70	1·85	4·53	2·77
2585	3·87	1·80	4·92	2·91
2200	4·20	1·81	5·20	2·77
1950	4·83	2·12	5·74	2·99
1700	4·74	1·78	6·00	2·85
1370*	5·40	1·86	6·75	2·90
1250*	6·00	2·10	7·00	2·85
600*	8·48	2·00	9·84	2·70

* Measurements obtained on a 2 ft. diameter disk.

$R_r = r^2\omega/\nu$.

A few check observations were made at this stage with a double-sized disk, of 24 in. diameter. As the same Reynolds number at transition was obtained as on the smaller disk, it was assumed that the flow was not influenced by the finite size of the disk. The large disk was not used further as it was imperfectly balanced and could not be spun at high speeds.

6. VELOCITY TRAVERSES ON THE DISK

Figure 5 illustrates the co-ordinates and velocity components which describe the flow on the rotating disk. Two series of velocity traverses through the boundary layer at a number of different radii in the laminar, instability and turbulent regions were taken at rotational speeds of 2100 and 2700 rev/min. The experimental observations are plotted in figures 6 and 7.

While the boundary layer remains laminar, the theoretical independence of boundary-layer thickness and radius is seen to be satisfied. The comparison with the theoretical laminar profile is also shown in figure 8, where the traverses in the stable laminar region at the two speeds are plotted together in non-dimensional form. The curve of resultant velocity

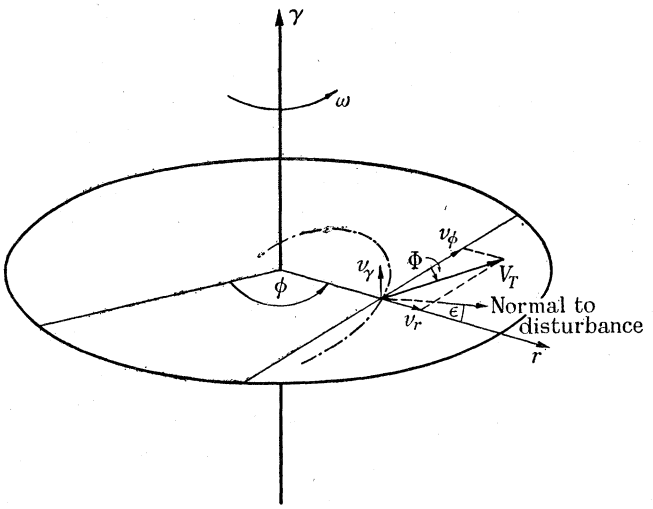

FIGURE 5. Rotating disk co-ordinates and velocity components. ·–·–, axis of disturbance vortex (logarithmic spiral of angle $\frac{1}{2}\pi+\epsilon$). $\zeta=\gamma\sqrt{(\omega/\nu)}$; $v_r=r\omega F(\zeta)$; $v_\phi=r\omega G(\zeta)$; $v_\gamma=\sqrt{(\nu\omega)}\,H(\zeta)$.

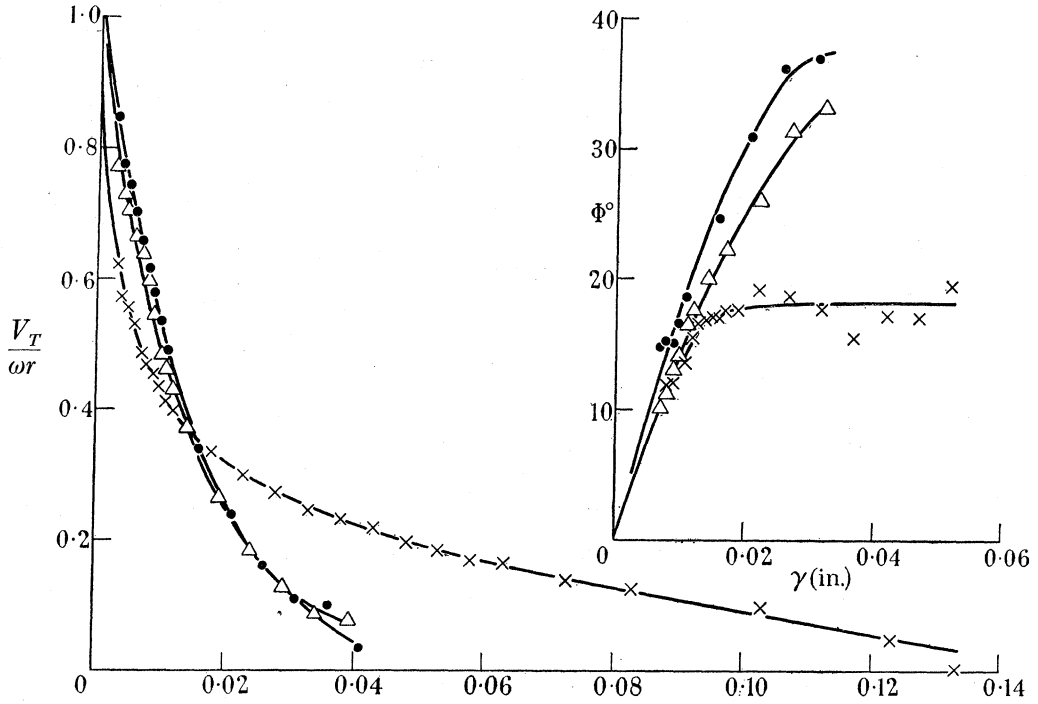

FIGURE 6. Experimental boundary-layer traverses on disk at 2100 rev/min. Under these conditions, instability occurs at 4·14 in. and transition at 5·28 in.

experimental point	•	△	×
radius of traverse (in.)	3·75	4·75	5·75

shows very good agreement with theory, but the curve of the direction of flow is less satisfactory. As previously suggested, it is thought that the discrepancies are due to experimental errors in measurement rather than to a real departure of the flow from the theoretical predictions. As a result of this discrepancy in angle, when the velocity profile is resolved into components in the tangential and radial directions (figures 9 and 10), it is found that, for laminar flow, the tangential component is in good agreement with theory, whilst the radial component has a peak value which is somewhat short of the theoretical.

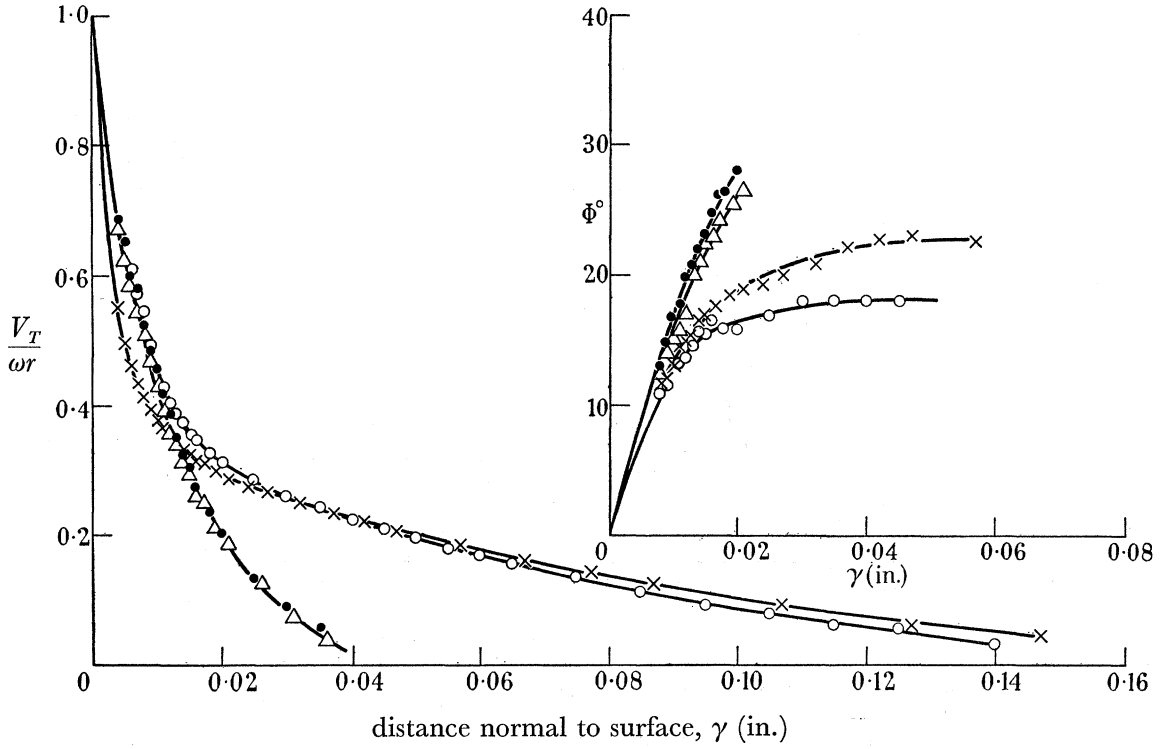

FIGURE 7. Experimental boundary-layer traverses on disk at 2700 rev/min. Under these conditions, instability occurs at 3·7 in. and transition at 4·8 in.

experimental point	•	△	○	×
radius of traverse (in.)	3·0	4·0	5·2	5·75

It is interesting to compare the measured turbulent profile with the profiles that have been assumed by theoretical investigators in attempts to calculate the resistance of the disk to rotation. The derivation of von Kármán's (1921) one-seventh power profile and of Goldstein's (1935) logarithmic profile are both described by the latter author.

Von Kármán (1921) assumes

$$v_\phi = r\omega[1-(\gamma/\delta)^{\frac{1}{7}}] \quad \text{and} \quad v_r = \alpha r\omega(\gamma/\delta)^{\frac{1}{7}}[1-\gamma/\delta],$$

where $\gamma = \delta$ is taken as the edge of the boundary layer and $\cot^{-1}\alpha$ is the angle that the flow relative to the surface makes with the radius vector close to the surface. The value $\alpha = 0{\cdot}162$ is obtained when the distributions given above are substituted in the momentum integral equation and solved with the power skin-friction formula

$$\tau_0 = 0{\cdot}0225\rho U^2\left(\frac{\nu}{U\delta}\right)^{\frac{1}{4}}, \quad \text{where} \quad U = (1+\alpha^2)^{\frac{1}{2}} r\omega.$$

Goldstein (1935) assumes a logarithmic law for the shearing stress at the wall, and has to express his radial velocity profile in two portions. The formulae are

$$v_r = -\frac{r\omega}{Y}\ln(\gamma/\delta)$$

and

$$v_\phi = \alpha r\omega\left[1+\frac{1}{Y}\ln\gamma/\delta\right] \quad \text{for} \quad \gamma/\delta<(\gamma/\delta)_1;$$

$$v_\phi = -\frac{\alpha r\omega}{Y}\ln\gamma/\delta \quad \text{for} \quad (\gamma/\delta)_1<\gamma/\delta<1,$$

where $(\gamma/\delta) = \mathrm{e}^{-\frac{1}{2}Y}$, $\alpha = \frac{1}{3}$ and $R_r\,(=r^2\omega/\nu) = 0{\cdot}826Y\,\mathrm{e}^{Y}$.

These formulae lead to values of the angles of yaw ϕ at the outside edge of the boundary layer of 48° 36′ for von Kármán's profile and 18° 30′ for Goldstein's profile. The latter profile is thus in better agreement with the experimental values of 18 to 23° (figures 6 and 7).

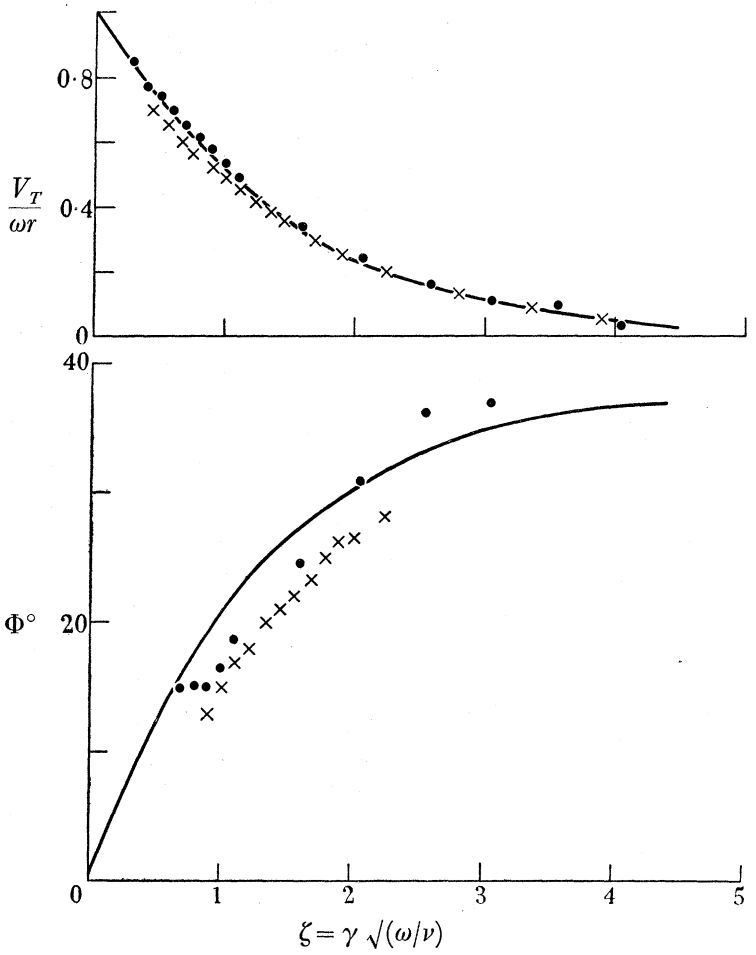

FIGURE 8. (*a*) Variation of resultant velocity through the laminar boundary layer.
(*b*) Variation of flow direction through the laminar boundary layer.

experimental point	•	×
rotational speed of disk ($=60\omega/2\pi$) (rev/min)	2100	2700
radius of b.l. traverse, r (in.)	3·75	3·00
Reynolds number, $R_r = \omega r^2/\nu$	137 000	113 000

——, theoretical laminar profile

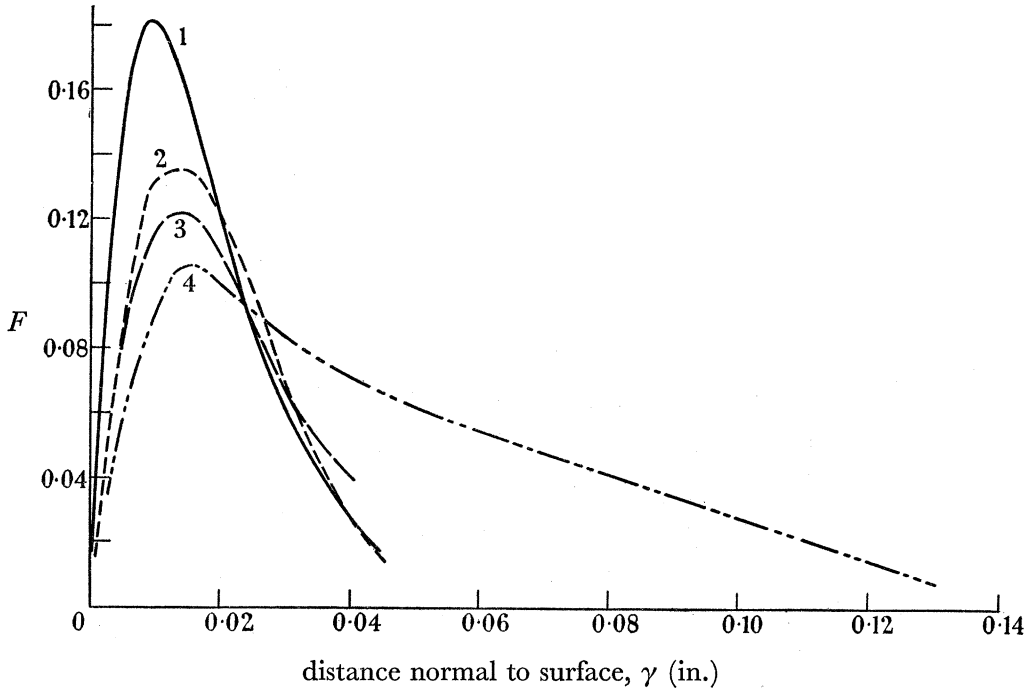

FIGURE 9. Radial components of experimental velocity profiles on disk at 2100 rev/min. Curve 1, theoretical laminar profile; 2, 3, 4 experimental profiles at various radii: 2, 3·75 in. (laminar); 3, 4·75 in. (instability region); 4, 5·75 in. (turbulent).

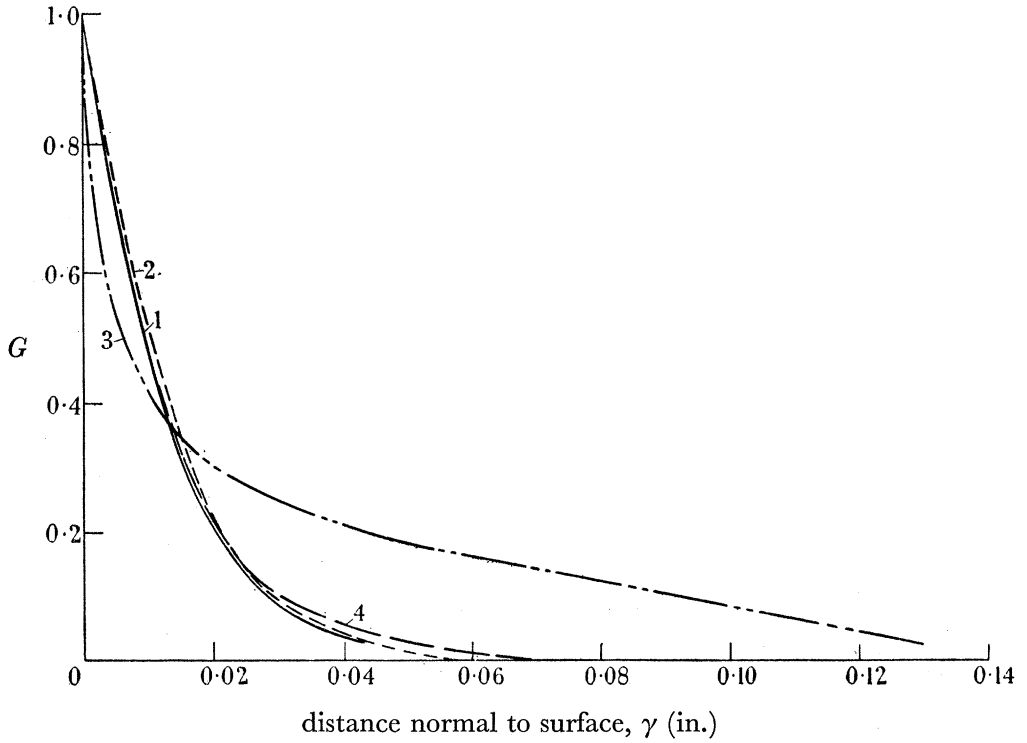

FIGURE 10. Tangential components of experimental velocity profiles on disk at 2100 rev/min. Curve 1, theoretical laminar profile; 2, 3, 4 experimental profiles at various radii: 2, 3·75 in. (laminar); 3, 4·75 in. (instability region); 4, 5·75 in. (turbulent).

Other comparisons are best seen from the graphs of the radial and tangential profiles plotted in figure 11 and compared with experiment at a Reynolds number of 323 000. The differences between the tangential components, G, are not very great, the experimental value of $H(\delta_1/\delta_2)$ being 1·4 compared with 1·29 for von Kármán's and 1·24 for Goldstein's profile. For the radial component, F, it will be seen that the maximum value and its position in the von Kármán profile are in good agreement with experiment, whereas the maximum

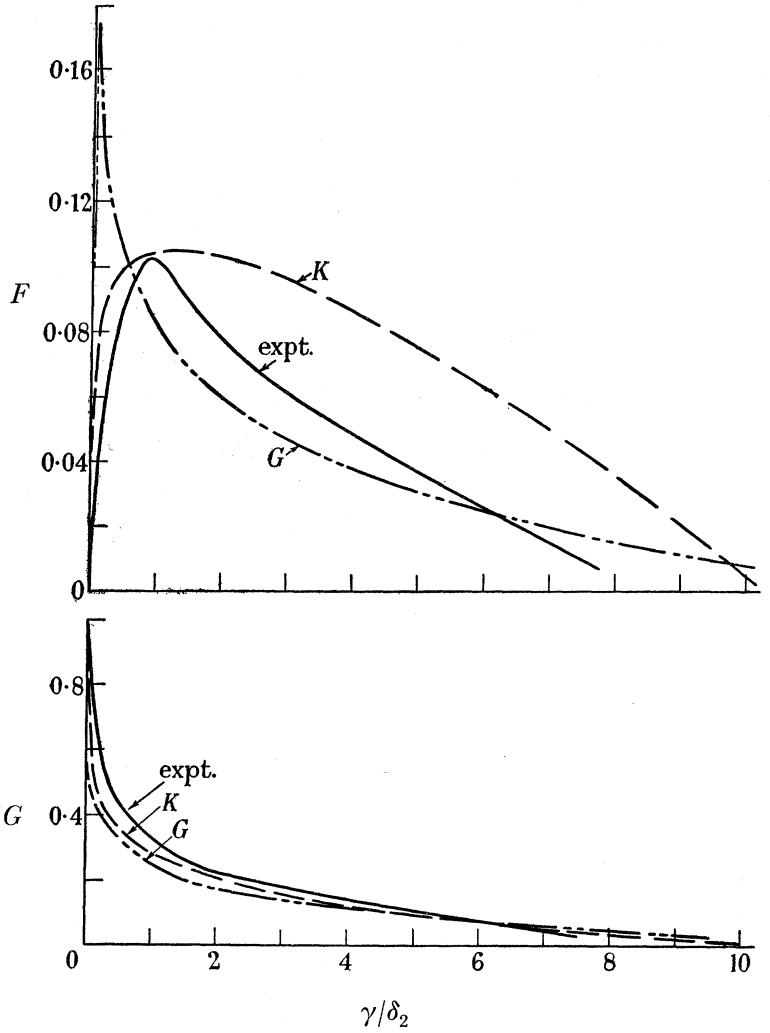

FIGURE 11. (*a*) Comparison of radial components of experimental and theoretical turbulent velocity profiles. (*b*) Comparison of tangential components of experimental and theoretical turbulent velocity profiles. K, von Kármán's profile; G, Goldstein's profile; expt., experimental profile. Radius of traverse = 5·75 in. $R_r\,(=r^2\omega/\nu) = 323\,000$. Value of R_r at transition = 285 000.

value of the logarithmic profile is much too high, and its position extremely close to the wall. On the other hand, Goldstein's logarithmic profile far away from the surface matches the experimental curve better than von Kármán's profile which has no point of inflexion.

Neither theoretical profile satisfactorily matches the experimental curve in all features, and this evidence suggests that it might be worth while to make a fresh attempt to formulate a more satisfactory analytical representation to the turbulent boundary-layer profile.

7. Experimental investigation of the instability on the disk

The measurements of the position of the onset of instability and of transition (table 1 and figure 4) by means of the china-clay technique and the aural stethoscope have already been referred to (§ 5). The present section investigates the instability region in greater detail.

It is interesting to note that the visualization technique employed is only capable of demonstrating the presence of stationary modes of disturbance. It was noteworthy that such disturbances were present so strongly on the rotating disk. The more complicated nature of the flow was suspected from a careful examination of the photographs such as figure 4. The vortex traces are not exactly regularly spaced, and some of them appear to fade in or out at different radii so that it proved difficult to say precisely how many were present round the circumference of the disk.

The difficulty was to some extent resolved by replacing the aural stethoscope by a moving-coil microphone fitted with a probe tube. This consisted of a short length of 0·05 in. bore hypodermic tubing, held in the boundary layer as a total head tube, connected to about $2\frac{1}{2}$ ft. of $\frac{1}{4}$ in. bore plastic tubing. The output from the microphone was amplified and analyzed by means of a narrow-band, feed-back-type analyzer,* and figure 12 shows the variation of noise analyses with differing radii for two rotational speeds of the disk (1500 and 2200 rev/min). The ordinates of the graphs are the actual amplifier readings, and no correction has been made for the frequency characteristics or the probe tube, microphone and amplifier.

At frequencies below 200 c/s, disturbances are detected in all sets of observations which are clearly connected with harmonics of the disk rotational speed, and this portion of the curves can be disregarded. At higher frequencies, low readings were obtained when the probe was 0·01 in. from the surface in the pure laminar layer where the radius was less than the critical radius for instability. This suggests that the considerably higher readings obtained when the probe was at larger radii are related to the velocity disturbances in the boundary layer. They are shown not to be due to motor or other extraneous noise, as low readings were again obtained when the probe was withdrawn to 0·25 in. from the surface so as to be entirely clear of the boundary-layer flow.

The traverses show that as the radius is increased and the probe enters the instability region, increased energy is found concentrated in a narrow frequency band. As the traverse moves into the region of turbulent flow, the output over the rest of the range of frequencies increases until the energy level is high throughout. The critical radii as previously measured on the china-clay picture are thus clearly indicated by the changes which occur in the shape of the frequency analysis diagram. Moreover, as the frequency band of growing disturbances is much broader than would be given by a single disturbance at some discrete frequency, it would appear that disturbances which are amplified are spread over a range of frequencies; for example, at a disk speed of 2200 rev/min the range is from about 900 to 1300 c/s, that is, from about 25 to 35 times the disk frequency. This same range, in terms of the disk frequency, is also found at the lower disk speed of 1500 rev/min.

* Acknowledgement is due to Mr W. C. T. Copeland of Physics Division, N.P.L., for the loan of acoustic apparatus and the benefit of his valuable advice.

PHILOSOPHICAL TRANSACTIONS OF THE ROYAL SOCIETY A MATHEMATICAL, PHYSICAL & ENGINEERING SCIENCES

Now there are probably several frequencies within the unstable band for which the disturbances have the same component of velocity in the tangential direction as the disk itself. The wave fronts of such disturbances will therefore appear stationary relative to the disk, and these are the disturbances which will record in the china-clay technique. The spacing of such disturbances (measured in the tangential direction) may be defined in terms of the apparent number of vortices on the disk and is then the ratio of the disturbance frequency to the disk frequency. The examples of figure 12 suggest that this ratio (which is equal to the number of stationary waves where such waves exist) lies between 25 and 35, with the

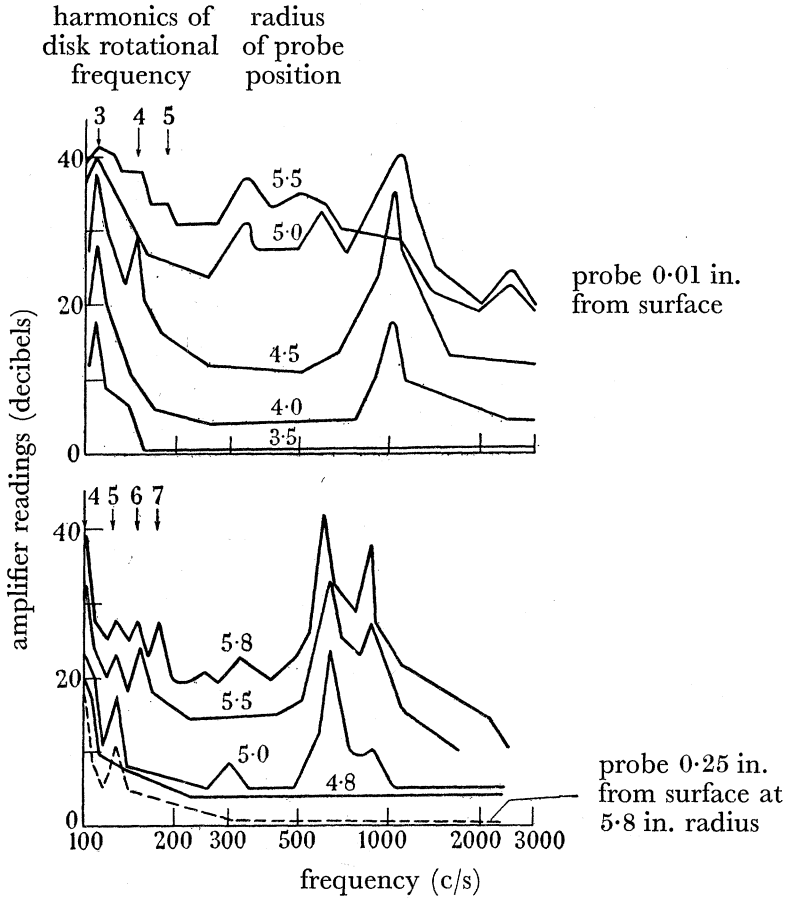

FIGURE 12. (*a*) Boundary-layer noise analysis on disk at 2200 rev/min.
(*b*) Boundary-layer noise analysis on disk at 1500 rev/min.

possibility of the strongest pattern at about 30. This is in agreement with the china-clay record which suggests the presence of between 28 and 31 vortices. The number cannot be precisely evaluated as the above discussion suggests that the china-clay pattern probably results from the superposition of a number of similar steady states, which would be expected to produce the observed slight modulations in strength and spacing. It is noteworthy that a pattern is obtained at all, as an integrated result of some 4 min not always very steady running; conceivably, the stationary vortices are 'locked' to the disk by the influence of minute roughness on the surface. The presence of one or more stationary wave systems does not preclude some of the frequencies in which energy is present (figure 12) from representing waves travelling relative to the disk, but this cannot be ascertained without additional

measurements (requiring hot-wire technique) of either wave-length or wave velocity, in which narrow bands of the frequency range are separately investigated with the aid of suitable filters. Alternatively, the probe could be fixed relative to the surface, as would be done in an investigation on a swept wing.

Smith's (1947) measurements with twin hot wires are of little assistance here. For although frequency, wave-length and direction of propagation were considered, the modulation present in the oscillograms of frequency was ignored, and so the result is only a mean. The possibility of there being wave fronts stationary relative to the disk was not apparently realized by Smith, and the measured values suggest a wave advancing in the tangential direction with $0{\cdot}2 \operatorname{cosec} 14^\circ = 0{\cdot}8$ of the disk velocity. But an error of only 2° in the measurement of the direction of propagation, or of 20 % in the value of the wave velocity, or smaller combinations of both, would be consistent with stationary wave fronts relative to the disk, so the evidence is inconclusive.

The direction of propagation of the waves as given by the china-clay picture is about 14° from the radial direction, and this is in agreement with Smith's result.

The theoretical explanation of the instability is given in part II below, where it is suggested that, in the absence of viscosity, and for neutral disturbances that are neither amplified nor damped, the number of stationary vortices on the disk would vary between 113 and 140 for the experimentally observed range of Reynolds numbers between the start of the instability and transition. This is about four times the experimental values, so viscosity evidently modifies the solution considerably. The angle that the direction of propagation makes with the radius is calculated as $13\frac{1}{4}^\circ$, which is in excellent agreement with the observed value of about 14°.

8. Conclusions from the experimental work

The present experiments on the flow over a rotating disk have disclosed the presence of a strong instability of the laminar boundary layer due, as in the analogous flow over a swept wing, to its three-dimensionality. Amplified waves arise which lead rapidly to transition of the flow. The waves cover a certain band of frequencies (measured at a point fixed in space) and some of the waves are found to be stationary relative to the surface of the disk, thus giving rise to the observed vortex pattern.

The laminar boundary-layer profile on the disk was found to be in agreement with theoretical calculation. The measured turbulent profile differed considerably from the assumptions that have previously been made to enable the resistance to rotation of the disk to be calculated. There is scope for further measurements over a range of Reynolds numbers and for the formulation of a better analytical representation of the turbulent profile.

Part II. Theoretical

By J. T. Stuart

9. The general equations of motion

In this section are examined the linearized equations which govern the growth of small periodic disturbances in a three-dimensional flow over a curved surface. Orthogonal curvilinear co-ordinates are used, α and β being the co-ordinates on the surface, and γ the co-ordinate normal to the surface. It is assumed that the disturbance of the flow is periodic

in the co-ordinate α, but this does not reduce the generality as the co-ordinates α, β are as yet unspecified.

The components of velocity corresponding to α, β, γ are u, v, w (in vector form $\mathbf{v}$); and the vorticity is ξ, η, ζ (in vector form $\boldsymbol{\omega}$). In addition, p denotes pressure, t time, ν kinematic viscosity, ρ density and μ viscosity.

Then the equations of motion for incompressible flow are (Goldstein 1938)

$$\frac{\partial \mathbf{v}}{\partial t} - \mathbf{v} \wedge \boldsymbol{\omega} = -\operatorname{grad}\left(\frac{p}{\rho} + \tfrac{1}{2}\mathbf{v}^2\right) + \nu(\operatorname{grad}\operatorname{div}\mathbf{v} - \operatorname{curl}\boldsymbol{\omega}), \tag{9·1}$$

$$\boldsymbol{\omega} = \operatorname{curl}\mathbf{v}, \tag{9·2}$$

and

$$\operatorname{div}\mathbf{v} = 0. \tag{9·3}$$

It is convenient, though not necessary, to retain the term in $\operatorname{grad}\operatorname{div}\mathbf{v}$ in (9·1). We choose a family of surfaces parallel to the given surface such that the co-ordinate γ represents the actual distance normal to the given surface (Howarth, 1951). The elements of length in directions α, β, γ are then

$$h_1 \mathrm{d}\alpha, \quad h_2 \mathrm{d}\beta, \quad \mathrm{d}\gamma, \tag{9·4}$$

that is,

$$\mathrm{d}s^2 = h_1^2 \mathrm{d}\alpha^2 + h_2^2 \mathrm{d}\beta^2 + \mathrm{d}\gamma^2, \tag{9·5}$$

where $\mathrm{d}s$ is the element of length. In general, h_1 and h_2 depend on α, β and γ, but are connected by certain (Lamé) relations (Howarth 1951).

We recall that the components of vorticity are

$$\left.\begin{aligned} \xi &= \frac{1}{h_2}\left\{\frac{\partial w}{\partial \beta} - \frac{\partial}{\partial \gamma}(h_2 v)\right\}, \\ \eta &= \frac{1}{h_1}\left\{\frac{\partial}{\partial \gamma}(h_1 u) - \frac{\partial w}{\partial \alpha}\right\}, \\ \zeta &= \frac{1}{h_1 h_2}\left\{\frac{\partial}{\partial \alpha}(h_2 v) - \frac{\partial}{\partial \beta}(h_1 u)\right\}, \end{aligned}\right\} \tag{9·6}$$

while

$$\operatorname{div}\mathbf{v} = \frac{1}{h_1 h_2}\left\{\frac{\partial}{\partial \alpha}(h_2 u) + \frac{\partial}{\partial \beta}(h_1 v) + \frac{\partial}{\partial \gamma}(h_1 h_2 w)\right\}, \tag{9·7}$$

and the components of gradient are

$$\frac{1}{h_1}\frac{\partial}{\partial \alpha}, \quad \frac{1}{h_2}\frac{\partial}{\partial \beta}, \quad \frac{\partial}{\partial \gamma}. \tag{9·7}$$

The vector product $\mathbf{v} \wedge \boldsymbol{\omega}$ has its usual component:

$$v\zeta - w\eta, \quad w\xi - u\zeta, \quad u\eta - v\xi. \tag{9·9}$$

The disturbance imposed on the main flow of velocity $\mathbf{V}$, vorticity $\boldsymbol{\Omega}$ and pressure P is given by

$$\left.\begin{aligned} \mathbf{v} &\equiv \mathbf{V} + \mathbf{v}_1 \mathrm{e}^{\mathrm{i}(n\alpha - \lambda t)} \equiv \mathbf{V} + \mathbf{v}_1', \\ \boldsymbol{\omega} &\equiv \boldsymbol{\Omega} + \boldsymbol{\omega}_1 \mathrm{e}^{\mathrm{i}(n\alpha - \lambda t)} \equiv \boldsymbol{\Omega} + \boldsymbol{\omega}_1', \\ p &\equiv P + p_1 \mathrm{e}^{\mathrm{i}(n\alpha - \lambda t)} \equiv P + p_1', \end{aligned}\right\} \tag{9·10}$$

where n is the (real) wave number, and λ the (complex) frequency. If it is found that disturbances can exist with the imaginary part of λ positive, the motion is unstable.

After substitution of (9·10) in (9·1), (9·2) and (9·3), and linearization for small disturbances, we obtain the following disturbance equations:

$$\left.\begin{aligned} -\mathrm{i}\lambda\mathbf{v}_1' - \mathbf{V}\wedge\boldsymbol{\omega}_1' - \mathbf{v}_1'\wedge\boldsymbol{\Omega} &= -\operatorname{grad}\left(\frac{p_1'}{\rho}+\mathbf{V}.\mathbf{v}_1'\right)+\nu(\operatorname{grad}\operatorname{div}\mathbf{v}_1' - \operatorname{curl}\boldsymbol{\omega}_1'),\\ \boldsymbol{\omega}_1' &= \operatorname{curl}\mathbf{v}_1',\\ \boldsymbol{\Omega} &= \operatorname{curl}\mathbf{V},\\ \operatorname{div}\mathbf{v}_1' &= 0. \end{aligned}\right\} \tag{9·11}$$

The equations (9·11) consist of four linear differential equations for the quantities $\mathbf{v}_1$ ($\equiv u, v, w$) and p; the equations contain also the main flow $\mathbf{V}$ ($\equiv U, V, W$) parameters λ and n and a reference velocity V_0.

We shall use the notation

$$\left.\begin{aligned} \mathbf{v}_1 &\equiv u, v, w;\\ \mathbf{V} &\equiv U, V, W;\\ \boldsymbol{\omega}_1 &= \xi_1, \eta_1, \zeta_1;\\ \boldsymbol{\Omega} &= \xi_0, \eta_0, \zeta_0. \end{aligned}\right\} \tag{9·12}$$

Then from (9·6)

$$\left.\begin{aligned} \xi_0 &= \frac{1}{h_2}\left\{\frac{\partial W}{\partial\beta} - \frac{\partial}{\partial\gamma}(h_2 V)\right\},\\ \eta_0 &= \frac{1}{h_1}\left\{\frac{\partial}{\partial\gamma}(h_1 U) - \frac{\partial W}{\partial\alpha}\right\}, \end{aligned}\right\} \tag{9·13}$$

and

$$\zeta_0 = \frac{1}{h_1 h_2}\left\{\frac{\partial}{\partial\alpha}(h_2 V) - \frac{\partial}{\partial\beta}(h_1 U)\right\},$$

while from (9·6) and (9·10)

$$\left.\begin{aligned} \xi_1 &= \frac{1}{h_2}\left\{\frac{\partial w}{\partial\beta} - \frac{\partial}{\partial\gamma}(h_2 v)\right\},\\ \eta_1 &= \frac{1}{h_3 h_1}\left\{\frac{\partial}{\partial\gamma}(h_1 u) - \frac{\partial w}{\partial\alpha} - \mathrm{i}nw\right\}, \end{aligned}\right\} \tag{9·14}$$

$$\zeta_1 = \frac{1}{h_1 h_2}\left\{\frac{\partial}{\partial\alpha}(h_2 v) + \mathrm{i}nh_2 v - \frac{\partial}{\partial\beta}(h_1 u)\right\}.$$

And

$$\begin{aligned} \operatorname{div}\mathbf{v}_1' &= \frac{1}{h_1 h_2}\left\{\frac{\partial}{\partial\alpha}(h_2 u) + \mathrm{i}nh_2 u + \frac{\partial}{\partial\beta}(h_1 v) + \frac{\partial}{\partial\gamma}(h_1 h_2 w)\right\}\exp[\mathrm{i}(n\alpha - \lambda t)]\\ &= Q\exp[\mathrm{i}(n\alpha - \lambda t)], \end{aligned} \tag{9·15}$$

the symbol Q being introduced for convenience.

The quantities of (9·12) and Q all depend on α, β and γ; and in general the same is true of h_1 and h_2. The velocity and vorticity functions are more sensitive to changes in γ than in α and β; that is, their derivatives with respect to α and β are of a lower order of magnitude than those with respect to γ. But the functions h_ν are equally sensitive to α, β and γ, because their derivatives represent geometrical and not fluid-motion properties.

If the pressure is eliminated from (9·11) and if the above substitutions are made, we obtain a system of three differential equations for u, v and w. The analysis is lengthy and is not given in detail.

Non-dimensional quantities used in the analysis are defined as follows:

$$\left.\begin{aligned} &\alpha = lx, \quad U = V_0\,\overline{U}, \quad \frac{\delta}{\mu}p_1 = p_2,\\ &\beta = ly, \quad V = V_0\,\overline{V},\\ &\gamma = \delta z, \quad W = \frac{\delta}{l}V_0\,\overline{W},\\ &\sigma = \frac{n\delta}{h_1}, \quad c = \frac{\lambda h_1}{nV_0},\\ &R = \frac{V_0\delta}{\nu},\\ &m_{12} = \frac{\delta}{h_1 h_2}\frac{\partial h_1}{\partial \beta}, \quad m_{21} = \frac{\delta}{h_1 h_2}\frac{\partial h_2}{\partial \alpha},\\ &m_{13} = \frac{\delta}{h_1}\frac{\partial h_1}{\partial \gamma}, \quad m_{23} = \frac{\delta}{h_2}\frac{\partial h_2}{\partial \gamma};\\ &\delta_1' = \frac{1}{h_1}\frac{\delta}{l}, \quad \delta_2' = \frac{1}{h_2}\frac{\delta}{l}, \quad \delta_3' = \frac{\delta}{l}. \end{aligned}\right\} \tag{9·16}$$

The quantity δ is a suitable measure of the boundary-layer thickness; it is a constant, and is a thickness associated with a particular point of the surface. And l is a length characteristic of the scale of the system, for example, the chord of an aerofoil or the local radius on a rotating disk. The variables x, y, z as defined are of the same order of magnitude, and account is taken of the small magnitude of W compared with U and V. The reference velocity, V_0, is the resultant velocity outside the boundary layer at a particular point; it is a constant.

Curvature of the surface is represented by m_{13} and m_{23}, and of the streamlines by m_{12} and m_{21}.

Since we are concerned with small curvature, h_1 and h_2 may be regarded as of order 1, and $\partial h_\mu/\partial\alpha$, etc., of order r^{-1}, where r is a typical radius of curvature. In general, δ/r and $m_{\nu\mu}$ are of order R^{-1}, R being the Reynolds number. Similarly δ_ν' $(\nu = 1, 2, 3)$ is of order R^{-1}.

In the analysis of the disturbance equations (9·11), terms of order 1 and R^{-1} are retained, and terms in R^{-2} are neglected. It is important to note that σ, c and R depend on x, y and z through h_ν.

The analysis yields the following three equations for the velocities:

$$\begin{aligned} &(\overline{U}-c)\left(\frac{\partial^2 w}{\partial z^2}-\sigma^2 w\right)-\frac{\partial^2\overline{U}}{\partial z^2}w+\frac{\mathrm{i}}{\sigma R}\left(\frac{\partial^4 w}{\partial z^4}-2\sigma^2\frac{\partial^2 w}{\partial z^2}+\sigma^4 w\right)\\ &\quad = m_{12}\left[c\frac{\partial v}{\partial z}+\frac{\mathrm{i}}{\sigma}\frac{\partial}{\partial z}\left(\overline{V}\frac{\partial w}{\partial z}\right)\right]+m_{13}\left[3(c-\overline{U})\frac{\partial w}{\partial z}+w\frac{\partial\overline{U}}{\partial z}\right]\\ &\qquad +m_{21}\left[\frac{\mathrm{i}}{\sigma}(c-\overline{U})\frac{\partial^2 w}{\partial z^2}-\frac{\mathrm{i}}{\sigma}\frac{\partial\overline{U}}{\partial z}\frac{\partial w}{\partial z}-2\frac{\partial}{\partial z}(v\overline{V})\right]+m_{23}\left[(c-\overline{U})\frac{\partial w}{\partial z}-w\frac{\partial\overline{U}}{\partial z}+2\mathrm{i}\sigma v\overline{V}\right]\\ &\qquad +\frac{\mathrm{i}}{\sigma}\delta_1'\left[c\left(\frac{\partial^3 w}{\partial x\,\partial z^2}+\sigma^2\frac{\partial w}{\partial x}\right)-2\sigma^2\overline{U}\frac{\partial w}{\partial x}+\frac{\partial\overline{U}}{\partial x}\left(\frac{\partial^2 w}{\partial z^2}-\sigma^2 w\right)+\frac{\partial^2\overline{U}}{\partial x\,\partial z}\frac{\partial w}{\partial z}\right]\\ &\qquad +\delta_2'\left[(c-\overline{U})\frac{\partial^2 v}{\partial y\,\partial z}-\frac{\partial\overline{U}}{\partial z}\frac{\partial v}{\partial y}+\frac{\mathrm{i}}{\sigma}\overline{V}\left(\frac{\partial^3 w}{\partial y\,\partial z^2}-\sigma^2\frac{\partial w}{\partial y}\right)+\frac{\mathrm{i}}{\sigma}\frac{\partial\overline{V}}{\partial z}\frac{\partial^2 w}{\partial y\,\partial z}+\frac{\partial}{\partial z}\left(v\frac{\partial\overline{U}}{\partial y}\right)\right]\\ &\qquad +\frac{\mathrm{i}}{\sigma}\delta_3'\left[\frac{\partial}{\partial z}\left\{\overline{W}\left(\frac{\partial^2 w}{\partial z^2}-\sigma^2 w\right)\right\}\right], \end{aligned} \tag{9·17}$$

PHILOSOPHICAL TRANSACTIONS OF THE ROYAL SOCIETY A MATHEMATICAL, PHYSICAL & ENGINEERING SCIENCES

$$(\overline{U}-c)\,v+\frac{\mathrm{i}}{\sigma R}\left(\frac{\partial^2 v}{\partial z^2}-\sigma^2 v\right)-\frac{\mathrm{i}}{\sigma}w\frac{\partial \overline{V}}{\partial z}$$

$$=\frac{2}{\sigma^2}m_{12}\,\overline{U}\frac{\partial w}{\partial z}+m_{21}\left(\frac{\mathrm{i}}{\sigma}\,\overline{U}v-\frac{1}{\sigma^2}\,\overline{V}\frac{\partial w}{\partial z}\right)+\frac{\mathrm{i}}{\sigma}m_{23}w\overline{V}+\delta_1'\left[\frac{\mathrm{i}}{\sigma}\,\overline{U}\frac{\partial v}{\partial x}-\frac{1}{\sigma^2}\frac{\partial w}{\partial z}\frac{\partial \overline{V}}{\partial x}\right]$$

$$+\frac{\mathrm{i}}{\sigma}\delta_2'\left[\frac{\partial}{\partial y}(v\overline{V})+(\overline{U}-c)\frac{\partial^2 w}{\partial y\,\partial z}+\frac{\partial w}{\partial z}\frac{\partial \overline{U}}{\partial y}-\frac{\partial w}{\partial y}\frac{\partial \overline{U}}{\partial z}-w\frac{\partial^2 \overline{U}}{\partial y\,\partial z}\right]+\frac{\mathrm{i}}{\sigma}\delta_3'\overline{W}\frac{\partial v}{\partial z} \qquad (9{\cdot}18)$$

and

$$\mathrm{i}\sigma u+\frac{\partial w}{\partial z}=-m_{21}u-\delta_1'\frac{\partial u}{\partial x}-m_{12}v-\delta_2'\frac{\partial v}{\partial y}-(m_{13}+m_{23})\,w. \qquad (9{\cdot}19)$$

In each equation the inviscid and explicit R^{-1} terms are grouped on the left-hand side, and the terms in curvature and in x- and y-dependence on the right. It should be emphasized here that the co-ordinates α and β are as yet unspecified. In order to examine stability against a particular type of disturbance, the co-ordinates should be selected so that the disturbance is periodic in one co-ordinate only.

10. The nature of the disturbance equations

(a) *Previous work*

The equations of the previous section are of a very general character, and include as particular case, equations which have been used for previous investigations of hydrodynamic stability.

(i) *Stability of parallel flows*

If the flow is two-dimensional ($v=\overline{V}=0$), if all curvatures are zero ($m_{\nu\mu}=0$), and if the dependence of the velocities on x is neglected, equation (9·17) yields the Orr–Sommerfeld equation, which is applicable to the stability of two-dimensional flows for two-dimensional disturbances:

$$(\overline{U}-c)\left(\frac{\partial^2 w}{\partial z^2}-\sigma^2 w\right)-\frac{\partial^2 \overline{U}}{\partial z^2}w+\frac{\mathrm{i}}{\sigma R}\left(\frac{\partial^4 w}{\partial z^4}-2\sigma^2\frac{\partial^2 w}{\partial z^2}+\sigma^4 w\right)=0. \qquad (10{\cdot}1)$$

In this case, w can be replaced by a stream function ϕ, since from (9·19)

$$\mathrm{i}\sigma u+\frac{\partial w}{\partial z}=0.$$

That is,

$$u=\frac{\partial \phi}{\partial z},\quad w=-\mathrm{i}\sigma\phi.$$

Squire's theorem (1933) that a two-dimensional flow is more stable for three- than for two-dimensional disturbances can be deduced from our differential equations by omission of the m and δ' terms and substitution of $\overline{U}=\overline{U}_0\cos\epsilon$, $\overline{V}=\overline{U}_0\sin\epsilon$, where ϵ is the angle between the flow and the direction of propagation of the disturbance and $\overline{U}_0$ is the main flow.

(ii) *Two-dimensional flows including streamwise variation*

If the flow is two-dimensional ($v = \overline{V} = 0$), and if all curvatures are zero ($m_{\nu\mu} = 0$), equation (9·17) yields Pretsch's (1941) stability equation, which includes derivatives in the direction of flow. Equation (9·18) vanishes identically and (9·19) becomes

$$\mathrm{i}\sigma u + \frac{\partial w}{\partial z} = -\delta' \frac{\partial u}{\partial x}, \quad \text{where} \quad \delta' = \delta_1' = \delta_2' = \delta_3',$$

that is,

$$u = \frac{\partial \phi}{\partial z}, \quad w = \mathrm{i}\sigma\left(\phi - \frac{\mathrm{i}}{\sigma}\delta' \frac{\partial \phi}{\partial x}\right),$$

ϕ being a stream function.

Substitution into (9·17) and neglect of terms of order R^{-2} yields the equations (cf. Pretsch 1941)

$$(\overline{U} - c)\left(\frac{\partial^2 \phi}{\partial z^2} - \sigma^2 \phi\right) - \frac{\partial^2 \overline{U}}{\partial z^2}\phi + \frac{\mathrm{i}}{\sigma R}\left(\frac{\partial^4 \phi}{\partial z^4} - 2\sigma^2 \frac{\partial^2 \phi}{\partial z^2} + \sigma^4 \phi\right)$$
$$= \frac{\mathrm{i}}{\sigma}\delta'\left[\overline{W}\left(\frac{\partial^3 \phi}{\partial z^3} - \sigma^2 \frac{\partial \phi}{\partial z}\right) - \frac{\partial^2 \overline{W}}{\partial z^2}\frac{\partial \phi}{\partial z} + \left(2\sigma^2 c - 3\sigma^2 \overline{U} - \frac{\partial^2 \overline{U}}{\partial z^2}\right)\frac{\partial \phi}{\partial x} + \overline{U}\frac{\partial^3 \phi}{\partial x \partial z^2}\right], \quad (10{\cdot}2)$$

when use is made of the continuity condition of the main flow:

$$\frac{\partial \overline{U}}{\partial x} + \frac{\partial \overline{W}}{\partial z} = 0.$$

(iii) *Taylor–Görtler instability*

For two-dimensional flow on a curved surface with disturbances periodic across the stream, $\overline{U} = 0$ and derivatives with respect to x and y are neglected; that is, the terms in δ' are zero.

Let us examine the quantities $m_{\nu\mu}$. Now the element $\mathrm{d}s$ for cylindrical polar co-ordinates r, θ, α is given by

$$\mathrm{d}s^2 = \mathrm{d}r^2 + r^2 \mathrm{d}\theta^2 + \mathrm{d}\alpha^2. \quad (10{\cdot}3)$$

The fluid motion is in the direction of θ increasing, the co-ordinate normal to the surface is r and the disturbances are periodic in α. Let a be the constant radius of curvature of the surface, and define

$$\left.\begin{aligned} r &= a - \gamma, \\ a\theta &= \beta, \end{aligned}\right\} \quad (10{\cdot}4)$$

where the curvature is positive for a concave surface.

Equation (10·3) becomes

$$\mathrm{d}s^2 = \mathrm{d}\gamma^2 + \left(1 - \frac{\gamma}{a}\right)^2 \mathrm{d}\beta^2 + \mathrm{d}\alpha^2, \quad (10{\cdot}5)$$

and comparison with (9·5) gives

$$h_1 = 1, \quad h_2 = 1 - \frac{\gamma}{a}.$$

The only non-zero m is seen from (9·16) to be

$$m_{23} = \frac{1.\delta}{\left(1 - \frac{\gamma}{a}\right).1}\left(-\frac{1}{a}\right), \quad \sim -\frac{\delta}{a} \quad (10{\cdot}6)$$

for small values of δ/a. Since we have neglected streamwise variations, δ and m_{23} are constant.

With the substitutions

$$\sigma^2 - \mathrm{i}c\sigma R = \tau^2,$$
$$v = Rv_1, \quad w = w_1, \quad u = u_1,$$

and with neglect of one or two small terms, the equations (9·17), (9·18) and (9·15) become

$$\left.\begin{aligned} \frac{\partial^4 w_1}{\partial z^4}-(\sigma^2+\tau^2)\frac{\partial^2 w_1}{\partial z^2}+\sigma^2\tau^2 w_1 &= -2\sigma^2\frac{\delta}{a}R^2 v_1\overline{V}, \\ \frac{\partial^2 v_1}{\partial z^2}-\tau^2 v_1-w_1\frac{\partial \overline{V}}{\partial z} &= 0, \\ \mathrm{i}\sigma u_1+\frac{\partial w_1}{\partial z} &= 0. \end{aligned}\right\} \tag{10·7}$$

The fact that v is of larger order of magnitude than u and w is fundamental, and is referred to later.

The first two equations are the ones used by Görtler (1940*a*), and the third shows that u_1 is $\frac{1}{2}\pi$ out of phase with w_1 and v_1; Görtler's continuity equation is formally different from that above, since he correctly *assumes* real disturbances.

(iv) *Axial flow between rotating cylinders*

Goldstein (1937) has examined the stability of fluid flow under pressure along an annular pipe when the inner wall rotates. The analysis of our equations for this case corresponds to that of (iii) above, except that the velocity $\overline{U}$ in the α-direction is retained. Thus

$$\left.\begin{aligned} \frac{\partial^4 w_1}{\partial z^4}-[(\sigma^2+\tau^2)+\mathrm{i}\sigma R\overline{U}]\frac{\partial^2 w_1}{\partial z^2}+[\sigma^2\tau^2+\mathrm{i}\sigma R\overline{U}]w_1+\mathrm{i}\sigma R\frac{\partial^2\overline{U}}{\partial z^2}w_1 &= -2\sigma^2\frac{\delta}{a}R^2 v_1\overline{V}, \\ \frac{\partial^2 v_1}{\partial z^2}-[\sigma^2+\tau^2+\mathrm{i}\sigma R\overline{U}]v_1 &= w_1\frac{\partial\overline{V}}{\partial z} \\ \mathrm{i}\sigma u_1+\frac{\partial w_1}{\partial z} &= 0. \end{aligned}\right\} \tag{10·8}$$

These equations are more general than Goldstein's, since he considered a parabolic flow for $\overline{U}$, and the standard rotating-cylinder solution for $\overline{V}$. The Reynolds number R is $V_0\delta/\nu$, where V_0 is a standard velocity and δ the annular distance between the cylinder. The velocity V_0 is suitably taken as the velocity of the inner cylinder; Goldstein considered only very small axial Reynolds number, that is, $\overline{U}\ll\overline{V}$.

The above examples illustrate types of instability which have been considered on the basis of equations which may be deduced from the general equations (9·17) to (9·19). It will be noticed that the left-hand side of equation (9·17) is of a form associated with stability of two-dimensional flows, the velocity $\overline{U}$ which appears in (9·17) being the component in the direction of propagation of the disturbances. It is, of course, important to know the influence of the terms on the right-hand side of equations (9·17) to (9·19). Let us look at the examples cited. Pretsch (1941) has shown that the terms in δ' in equation (10·2) are unimportant for the stability problem, so that one needs to consider only the actual velocity profile, its change with surface distance being negligible. This reduces the stability of two-dimensional flows with pressure drop or rise to the solution of the Orr–Sommerfeld equation (10·1). In the Görtler equation (10·7), the terms in m_{23} are actually of dominating importance, and produce stability on convex and instability on concave walls.

In Görtler's case the disturbance velocity v in the direction of flow, being of higher order than u and w by a Reynolds number factor (R), raises the importance in (9·17) of the terms in m_{23}. This relation between v and w can be seen from (9·18) with $\overline{U}=0$ and $c=\mathrm{i}\beta/\sigma R$;

the dominating terms show that v is of order R times w, while (9·19) yields u of the same order as w. The physical realization of this important relation lies in the form of the Görtler parameter $R^2\delta/a$. The influence of the curvature terms in (9·17) is naturally less in cases where u, v and w are of the same order of magnitude.

For example, if $\overline{U}$ is not zero but is of substantial magnitude compared with $\overline{V}$, (9·18) shows that v and w are of similar order, while (9·19) again shows that u and w are of similar magnitude. Thus the m_{23} terms of (9·17) have not the same dominating influence; therefore as the magnitude of $\overline{U}$ increases one expects the flow to be stabilized; this is confirmed by Fage's (1938) experiments on the stability of axial flow between rotating cylinders (see Goldstein (1937) also).

(*b*) *The present investigation*

It is now proposed to discuss the stability of boundary-layer flows on plane or convex surfaces; in other words, the possibility of the Taylor–Görtler centrifugal type of instability is excluded. We shall be concerned with three-dimensional flows; but we note that Görtler's (1940*b*) work shows that surface curvature has little influence on stability of two-dimensional flows for two-dimensional disturbances.

In the flows to be considered, $\overline{U}$, $\overline{V}$ and $\overline{W}$ are all finite and non-zero. It is convenient to omit the surface curvature, since it is found that the type of instability considered appears for both plane and convex surfaces. From this restriction it follows that

$$m_{13} = m_{23} = 0,$$

that is, h_1 and h_2 are independent of γ ($\equiv z$), the distance normal to the surface. The obvious physical flow which exactly satisfies these conditions is that due to a rotating disk.

It has already been noticed that σ, R and c depend on x, y and z as in (9·16); but with the above restriction, the quantities σ, R and c are independent of the co-ordinate z. This is important because in the dominating terms of (9·17) to (9·19) (the left-hand sides) only derivatives with respect to z occur. Similarly, the δ'_ν quantities are independent of z.

We must now return to a consideration of the relative orders of magnitude of u, v and w, and in doing so we shall find a fundamental difference between our equations and those of Görtler (1940*a*). In cases to be considered here, the maximum of $\overline{U}$ ranges from about one-tenth to one-fifth of $\overline{V}$; thus in (9·18) the terms in $(\overline{U}-c)\,v$ is much larger than that in $\mathrm{i}/\sigma R$. It follows that v and w are of approximately the same order of magnitude and differ by a factor of order ten, which is much less than the Reynolds number factor difference between v and w in Görtler's case. Equation (9·19) shows that u and w are of the same order of magnitude in our case as well as in Görtler's. The upshot of this is that of the m terms of (9·17), those proportional to v have nothing like the dominating influence which they have in Görtler's work. When all the terms in m and δ' are neglected, the resulting system of equations is

$$(\overline{U}-c)\left(\frac{\partial^2 w}{\partial z^2}-\sigma^2 w\right)-\frac{\partial^2 \overline{U}}{\partial z^2}w+\frac{\mathrm{i}}{\sigma R}\left(\frac{\partial^4 w}{\partial z^4}-2\sigma^2\frac{\partial^2 w}{\partial z^2}+\sigma^4 w\right)=0, \tag{10·9}$$

$$(\overline{U}-c)\,v+\frac{\mathrm{i}}{\sigma R}\left(\frac{\partial^2 v}{\partial z^2}-\sigma^2 v\right)-\frac{\mathrm{i}}{\sigma}w\frac{\partial \overline{V}}{\partial z}=0, \tag{10·10}$$

$$\mathrm{i}\sigma u+\frac{\partial w}{\partial z}=0. \tag{10·11}$$

Since only derivatives with respect to z occur, this is a set of ordinary differential equations.

In an appendix, it is shown that although the m and δ' terms of (9·17) to (9·19) are of order R^{-1}, only the terms given above can be expected to affect stability in a local region. This is done by obtaining the solutions of (9·17) in terms of viscous and inviscid integrals. If expansions of the form given in the appendix are valid in a local region, so is the system of differential equations.

The boundary conditions for equations (10·9) to (10·11) are

$$u = v = w = 0 \quad \text{for} \quad z = 0$$

and

$$u, v, w \to 0 \quad \text{for} \quad z \to \infty.$$

But (10·11) shows that these can be replaced by

$$v = w = \partial w/\partial z = 0 \quad \text{at} \quad z = 0$$

and

$$v, w, \partial w/\partial z \to 0 \quad \text{as} \quad z \to \infty.$$

These boundary conditions with the equations determine an eigen-relation for σ, c and R. In fact the eigenvalues are determined by (10·9) with its four relevant boundary conditions. Then (10·10) with its two conditions gives v, w being now known; and (10·11) gives u.

Thus, in a localized region of a three-dimensional boundary layer, the velocity component in the direction of propagation of the disturbance may be regarded as a two-dimensional flow for stability purposes, and the usual two-dimensional stability theory applied. Disturbances propagated in different directions give different critical Reynolds numbers; but one expects that there is a unique lowest critical Reynolds number, corresponding to a particular disturbance pattern.

As yet, we have not considered the nature of disturbances which may be propagated in a three-dimensional flow; this is discussed in the next two sections.

11. The form of the boundary-layer velocity distribution

It is known that viscous and inflexional instability of flow is very much dependent on the velocity $\bar{U}$ which appears in the disturbance equation (9·9). In previous work on two-dimensional stability, attention has been directed to $\bar{U}$ functions which are of one sign only; for example, Heisenberg (1924), Tollmien (1929) and others have considered boundary-layer flows, flows between parallel and divergent planes, and jet and wake flows. For $\bar{U}$ functions of one sign, Tollmien (1935) has established necessary and sufficient conditions for instability, namely, that the profile $\bar{U}$ should have a point of inflexion. Near to this point of inflexion, the flow is of an unstable configuration, and causes disturbances to be generated.

In the present paper we are concerned primarily with $\bar{U}$ velocity functions which do change sign. To be specific, let us consider the velocity distribution in the boundary layer of a yawed infinite cylinder.

An academic but illustrative example which has been calculated—by Sears (1948) and by Schubart (see Schlichting 1951)–is the boundary layer corresponding to a potential flow which has a constant component of velocity parallel to the leading edge, and a component of velocity to the leading edge which increases linearly with distance. In such a boundary layer there are components of velocity both parallel to and normal to the leading edge. Now we can resolve these velocity components at a particular point parallel to and

normal to the potential streamline outside the boundary layer.* The component parallel to the potential streamline is of the ordinary boundary-layer form, whereas the normal

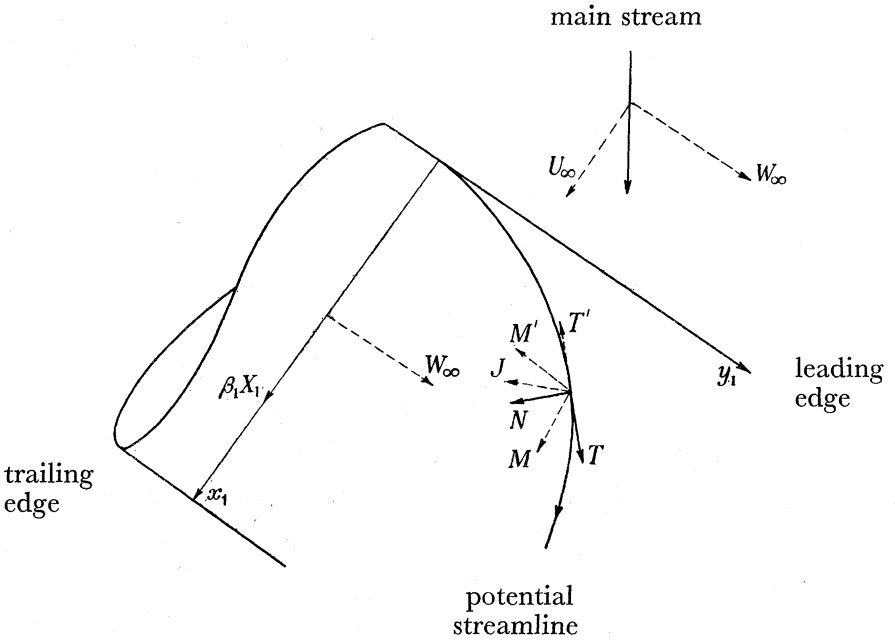

FIGURE 13. Yawed infinite cylinder.

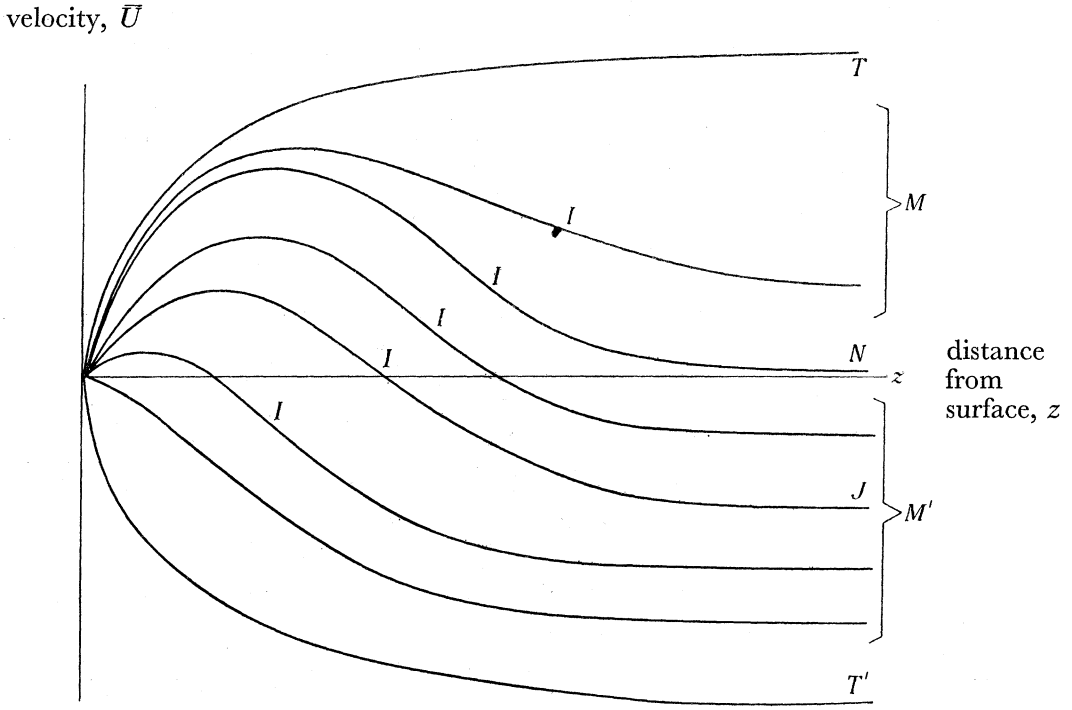

FIGURE 14. Components of velocity. ($I \equiv$ point of inflexion.)

component is zero at the wall and tends to zero at the edge of the boundary layer. For any other direction, the velocity profile is a combination of these two extreme (that is, tangential and normal) cases.

* The author is indebted to Professor H. B. Squire for this suggestion, which has been made independently by Owen and Randall (to be published).

Figure 13 shows a suitable co-ordinate system for a yawed infinite cylinder. In the diagram, T denotes the tangential direction, T' its reverse, N the normal direction, M a direction between T and N, and M' a direction between T' and N. A representative class of velocity profiles for the range of directions between T and T' is given in figure 14. The letters I denote the points of inflexion; the occurrence of a point of inflexion in the T and T' profiles depends, of course, on the velocity distribution outside the boundary layer. The size of the velocity component (N) (in figure 14) normal to the potential streamlines has been magnified compared with the tangential profile (T) for diagrammatic convenience.

The N-profile is zero at both ends of the range, and profiles within the M set are always positive, tending to T as the tangential direction is approached. Of the M' set of profiles, those nearer to N change sign, but those nearer to T' are negative. We note in passing that there is a particular M' profile for which the point of inflexion occurs at the point of zero velocity; this is denoted by J.

For the rotating disk (figure 5), it is convenient to consider velocities relative to the surface; that this is a valid step of a stability theory with curvature neglected can be seen from (10·9). In this case also, the curves of figure 14 are applicable in their general character; here the normal or N direction is along the radius.

12. Theorems concerning stability at infinite Reynolds number

We have shown that the determination of the eigenvalues σ, c, etc., depends on the equation (10·9); but if viscosity is neglected the equation becomes

$$(\bar{U}-c)\left(\frac{\partial^2 w}{\partial z^2}-\sigma^2 w\right)-\frac{\partial^2 \bar{U}}{\partial z^2}w=0, \tag{12·1}$$

subject to the conditions

$$w=0 \quad \text{at} \quad z=0$$

and

$$w, \frac{\partial w}{\partial z}\to 0 \quad \text{as} \quad z\to\infty. \tag{12·2a}$$

Outside the boundary layer, $\bar{U}$ is constant and $w\sim\exp(-\sigma z)$; thus the boundary conditions can be replaced by

$$\left.\begin{aligned} w&=0 \quad \text{at} \quad z=0\\ w'+\sigma w&=0 \quad \text{at} \quad z=z_\delta,\end{aligned}\right\} \tag{12·2b}$$

where primes denote differentiation with regard to z, and z_δ represents the edge of the boundary layer.

For neutral oscillations ($c=c_r+ic_i$, $c_i=0$), $\bar{U}-c$ must vanish at least one position, between the limits of integration. The proof given by Tollmien (1935) is applicable to any one of the profiles of figure 14. For several of the profiles given there, $\bar{U}=c$ not only at one point, but at two. These zeros of $(\bar{U}-c)$ constitute singularities of the equation (12·1); of course these singularities are not present in (9·9), but are introduced by the neglect of terms in R^{-1}. The solution of equation (12·1) is based upon the points z_1 and z_2, where $\bar{U}=c$, z_1 being the point for which $\bar{U}'$ is positive and z_2 that for which it is negative.

PHILOSOPHICAL TRANSACTIONS OF THE ROYAL SOCIETY A MATHEMATICAL, PHYSICAL & ENGINEERING SCIENCES

By using the method of Frobenius, we obtain formally the two independent solutions near $z = z_1$ in the form

$$\left.\begin{aligned} w_1^{(1)} &= (z-z_1)+a_2(z-z_1)^2+a_3(z-z_1)^3+\ldots, \\ w_2^{(1)} &= 1+b_1(z-z_1)+b_2(z-z_1)^2+b_3(z-z_1)^3+\ldots \\ &\quad +\frac{\bar{U}_1''}{\bar{U}_1'}w_1^{(1)}(z-z_1)\ln(z-z_1) \quad (z>z_1). \end{aligned}\right\} \tag{12·3}$$

An analysis of the viscous terms of (9·9), as was done by Tollmien and others, shows that

$$\ln(z-z_1) \sim \ln|z-z_1| - \pi i \quad \text{for} \quad z<z_1. \tag{12·4}$$

In the above formulae $\bar{U}_1'$, $\bar{U}_1''$ denote the first and second derivatives at $z = z_1$.

By expansion about $z = z_2$, similar solutions can be obtained:

$$\left.\begin{aligned} w_1^{(2)} &= (z-z_2)+c_2(z-z_2)^2+c_3(z-z_2)^3+\ldots, \\ w_2^{(2)} &= 1+d_1(z-z_2)+d_2(z-z_2)^2+d_3(z-z_2)^3+\ldots \\ &\quad +\frac{\bar{U}_2''}{\bar{U}_2'}w_1^{(2)}(z-z_2)\ln(z_2-z) \quad (z<z_2), \end{aligned}\right\} \tag{12·5}$$

$\bar{U}_2'$, $\bar{U}_2''$ denoting the first and second derivatives at $z = z_2$. Analysis shows that

$$\ln(z_2-z) \sim \ln|z-z_2| - \pi i \quad \text{for} \quad z>z_2 \tag{12·6}$$

(cf. stability theory of two-dimensional parallel flows (Lin 1945)).

Thus, we obtain the general solutions near to z_1 as

$$\left.\begin{aligned} w &= A_1 w_1^{(1)}+B_1 w_2^{(1)} \quad (z>z_1), \\ w &= A_1 w_1^{(1)}+B_1 w_2^{(1)}-B_1\frac{\bar{U}_1''}{\bar{U}_1'}w_1^{(1)}(z-z_1)\,\pi i \quad (z<z_1), \end{aligned}\right\} \tag{12·7}$$

A_1 and B_1 being (complex) constants.

Similarly, near to z_2

$$\left.\begin{aligned} w &= A_2 w_1^{(2)}+B_2 w_2^{(2)} \quad (z<z_2), \\ w &= A_2 w_1^{(2)}+B_2 w_2^{(2)}-B_2\frac{\bar{U}_2''}{\bar{U}_2'}w^{(2)}(z-z_2)\,\pi i \quad (z>z_2), \end{aligned}\right\} \tag{12·8}$$

A_2 and B_2 being (complex) constants.

In (12·7) and (12·8), the logarithms which occur in $w_2^{(1)}$ and $w_2^{(2)}$ are real.

Let us first consider a velocity profile with two critical points, z_1 and z_2, satisfying the conditions

$$z_1<z_2, \quad \bar{U}_1'>0, \quad \bar{U}_2'<0,$$

the boundaries being at $z = 0$ and $z = z_\delta$.

Noting Tollmien's work (1935), we consider the expression

$$\tau = w_i w_r' - w_r w_i', \tag{12·9}$$

which is proportional to the disturbance shearing stress ($-\rho\overline{uw} = -\rho\tau/2\sigma$). The suffixes r and i denote real and imaginary parts. By virtue of the boundary conditions (12·2), τ must be zero at $z = 0$ and $z = z_\delta$.

By substitution of (12·7) into (12·9), it can be shown that τ increases discontinuously by

$$-\frac{\bar{U}_1''}{\bar{U}_1'}\pi\,|\,B_1\,|^2 \tag{12·10}$$

at z_1 in going from $z<z_1$ to $z>z_1$.

Similarly, τ increases discontinuously by

$$-\frac{\bar{U}_2''}{\bar{U}_2'}\pi\,|\,B_2\,|^2 \tag{12·11}$$

at z_2 in going from $z>z_2$ to $z<z_2$.

Now, since (12·1) is a real differential equation, w_r and w_i must each be solutions of it. And further, from the properties of ordinary differential equations, we know that τ must be constant in a region without singularities. Therefore τ must take one constant value in the region $0<z<z_1$, another in the range $z_1<z<z_2$, and a third in the range $z_2<z<z_\delta$. But we know that, in the outer ranges, τ is zero; it follows immediately that

$$\frac{\bar{U}_1''}{\bar{U}_1'}\,|\,B_1\,|^2=\frac{\bar{U}_2''}{\bar{U}_2'}\,|\,B_2\,|^2, \tag{12·12}$$

where B_1 and B_2 are the values of w at the critical points z_1 and z_2 respectively. This condition is a *necessary* condition for the instability of a profile with two critical points.

If a value of c is chosen such that $(\bar{U}-c)$ has only one zero, then instead of (12·12) there is *one* of the relations

$$\left.\begin{aligned}\bar{U}_1''\,|\,B_1\,|^2&=0\quad(\bar{U}_1'>0),\\ \bar{U}_2''\,|\,B_2\,|^2&=0\quad(\bar{U}_2'<0).\end{aligned}\right\} \tag{12·13}$$

The first of these applies to profiles wholly positive, c being less than the limiting values of $\bar{U}$ at infinity; the second is applicable to profiles which change sign, c being negative.

Types of disturbance

We here consider the possible disturbances implicit in (12·12); for the velocity profiles of figure 14, $\bar{U}_1''\neq 0$, so that three cases arise, namely

$$\text{(i)}\quad B_1=0,\quad \bar{U}_2''=0,\quad B_2\neq 0, \tag{12·14}$$

$$\text{(ii)}\quad B_1=0,\quad B_2=0,\quad \bar{U}_2''\neq 0, \tag{12·15}$$

$$\text{(iii)}\quad \frac{\bar{U}_1''}{\bar{U}_1'}\,|\,B_1\,|^2=\frac{\bar{U}_2''}{\bar{U}_2'}\,|\,B_2\,|^2,\quad B_1\neq 0,\quad B_2\neq 0,\quad \bar{U}_2''\neq 0. \tag{12·16}$$

Case (i)

The condition $B_1=0$ shows that w is zero at the critical point $z=z_1$. By comparing a solution of (12·1) with one of

$$f''=\frac{\bar{U}''}{\bar{U}-c}f, \tag{12·17}$$

we can show that, in order to satisfy the boundary condition at the wall, c must be zero (cf. Tollmien 1935). Thus z_1 is zero and there is a critical point at the wall. It follows immediately that the profile $\bar{U}$ must be such that the point of inflexion lies at the point of zero velocity in the flow; there is *one* such profile (J) in figure 14—but see also figure 15 (a).

For this velocity profile, the existence of a non-zero wave number can be inferred as follows: the quantity $\bar{U}''/\bar{U}$ is everywhere negative, and equation (12·1) is here

$$w''+(-\sigma^2-\bar{U}''/\bar{U})\,w=0. \tag{12·18}$$

Let us compare a solution of (12·18) with one of

$$f''-j\bar{U}''/\bar{U}=0, \tag{12·19}$$

which has the same gradient as w at the wall. And let w and f both be zero at the wall (12·2b).

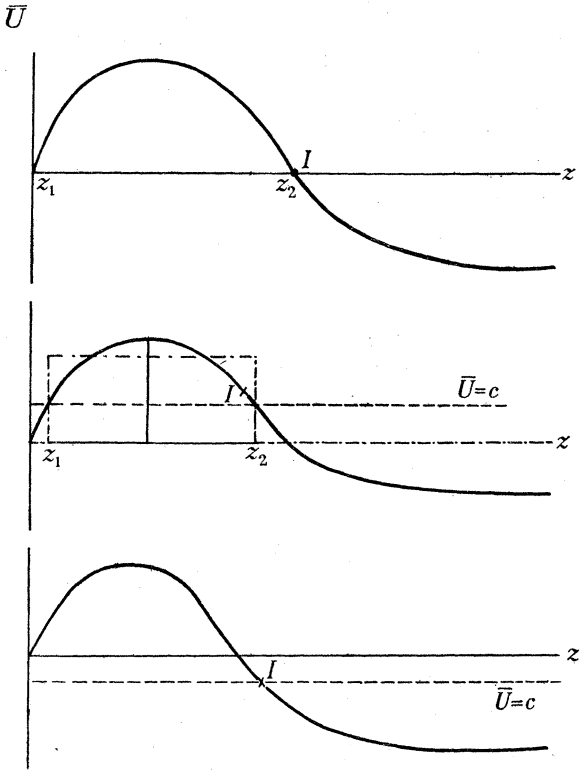

(a) Inviscid solution, $c=0$
Case (i) $\bar{U}_2''=0$ when $\bar{U}_2=0$
zero shearing stress
I = inflexion

(b) Inviscid solution, $c>0$
Case (iii). $-\cdot-\cdot-$, shearing stress $-\overline{\rho uw}\equiv-\dfrac{\rho}{2\sigma}\tau$

(c) Inviscid solution, $c<0$
single critical point; zero shearing stress.

FIGURE 15

Now an oscillation theorem of differential equations (Frank & Mises 1930) states that, since $(-\bar{U}''/\bar{U})$ is greater than $(-\sigma^2-\bar{U}''/\bar{U})$, w is greater than f up to the first zero of f. The required solution f is $f=\bar{U}$, which changes sign and has a finite limiting negative value at infinity. A suitably chosen value of σ^2 will ensure that w tends to zero at infinity.

It will be noted that the shearing stress is everywhere zero.

Case (ii)

As in (i), $B_1=0$ shows that c must be zero. The additional fact that $B_2=0$ leads to the degenerate vibration

$$w=\bar{U},\quad c=0,\quad \sigma^2=0,$$

which satisfies (12·2b). This type of vibration is applicable to any one of the profiles of figure 14.

Case (iii)

It is possible to determine limits to the value of c as follows. If the suffix I denotes the point of inflexion, figure 14 shows that $\overline{U}''<0$ for $z<z_I$ in the case of profiles with two critical points. Now since $\overline{U}_1'$ and $\overline{U}_2'$ are of opposite sign, $\overline{U}_1''$ and $\overline{U}_2''$ are of opposite sign (12·16). Immediately we can deduce that $z_2>z_I$ and $c<U_I$. The actual value of c cannot be obtained without proper solution of equation (12·1); the solution is complex (imaginary) because of the logarithmic transformations, the eigen-relation resulting from (12·2b) being sufficient to determine c and σ^2.

This type of disturbance is illustrated in figure 15b. The shearing stress is non-zero in the range z_1 to z_2, so that energy is transferred from one part of the flow to another. But the net energy transfer to the neutral disturbance is, of course, zero.*

Single critical point

For profiles with just one critical point, Tollmien's (1935) work is directly applicable. If the suffix I denotes the point of inflexion, c equals U_I and σ^2 is non-zero for the physically meaningful vibration, although there is also the degenerate vibration $c=0$, $\sigma^2=0$. In both cases the disturbance shearing stress is zero. These facts are summarized in figure 15c.

To summarize, in a three-dimensional boundary layer there is a continuous set of velocity profiles—corresponding to different directions—which are unstable. Most of the disturbances have a finite phase velocity, but there is one particular profile which generates a disturbance of zero phase velocity. The physical significance of these results is discussed in § 16.

13. A variational method of solution

Of the non-degenerate vibrations determined in the previous section, that for case (i) and that for the case of a profile with one critical point are such that the w solutions have no logarithmic singularities, and are entirely real. For such cases, the eigenvalue σ can be determined by a variational procedure.

Let us put

$$K(z)=-\overline{U}''/(\overline{U}-c); \tag{13·1}$$

then (12·1) becomes

$$w''-\sigma^2 w+K(z)\,w=0. \tag{13·2}$$

Multiplying by w, integrating and using (12·2a), we convert (13·2) to

$$\sigma^2=\int_0^\infty [K(z)\,w^2-w'^2]\,\mathrm{d}z\Big/\int_0^\infty w^2\,\mathrm{d}z, \tag{13·3}$$

where w satisfies the conditions (12·2a).

Now w is not known, but if a suitable function w is substituted into (13·3), a value for σ^2 results. It is now shown that if w is chosen so that (13·3) yields a maximum or minimum (i.e. extremal) value of σ^2, then such values of σ^2—if positive—are proper eigenvalues of equation (12·1).

Let us write

$$\sigma^2=I_1/I_2; \tag{13·4}$$

* A similar phenomenon has been noticed for unsymmetrical wakes and jets by Foote & Lin (1950).

then in the variational notation

$$\delta\sigma^2 = \frac{1}{I_2}(\delta I_1 - \sigma^2 \delta I_2). \tag{13·5}$$

Now

$$\delta I_1 = 2\int_0^\infty w\delta w\,\mathrm{d}z, \tag{13·6}$$

and by integration by parts

$$\delta I_2 = 2\int_0^\infty (K(z)\,w + w'')\,\mathrm{d}z. \tag{13·7}$$

Substituting (13·6) and (13·7) into (13·5), we have

$$\delta\sigma^2 = \frac{2}{I_2}\int_0^\infty (w'' + K(z)\,w - \sigma^2 w)\,\delta w\,\mathrm{d}z. \tag{13·8}$$

For an extremal value of σ^2, $\delta\sigma^2 = 0$; and since δw is an arbitrary variation, it follows that

$$w'' - \sigma^2 w + K(z)\,w = 0.$$

Therefore the condition that σ^2 of (13·3) takes an extremal value is that the original differential equation be satisfied. Immediately we can deduce that positive extremal values of σ^2 are proper eigenvalues.*

In practice, it is usually sufficient to choose a function which satisfies the boundary conditions, and which contains a single arbitrary constant. For case (i) of § 12, the singularity in $K(z)$ at $z = 0$ is counteracted by the zero in w in the integral relation (13·3).

The variational method developed in this section is applicable to the stability of two-dimensional flows whose profile contains a point of inflexion. For example, the exact solutions for a symmetrical, two-dimensional jet with symmetrical or anti-symmetrical disturbances (cf. Pai 1951) can be used to check this method and in fact the eigenvalues can be obtained to a very high degree of accuracy.

Fortunately, there is also an exact solution for a certain three-dimensional flow with which comparison can be made. Stuart (1954) has obtained the solution for the flow due to a rotating disk when there is large suction through the disk in the form

$$\left.\begin{aligned} F &= \frac{1}{2a^2}(\mathrm{e}^{-z} - \mathrm{e}^{-2z}), \\ G &= \mathrm{e}^{-z}, \end{aligned}\right\} \tag{13·9}$$

where $r\omega F$ is the radial velocity and $r\omega G$ the tangential velocity, r being the radius, ω the angular velocity and a the suction parameter. In this case $\delta = \delta_1$, the displacement thickness in the transformation (9·16); that is, $z = \gamma/\delta_1$. Now in a particular region of the boundary layer, let us find the component of velocity in a direction at an angle ϵ to the radius; the velocity is considered relative to the disk, as mentioned in § 11. The required component is (see figure 5)

$$r\omega[F\cos\epsilon - (1-G)\sin\epsilon],$$

while the dimensionless quantity $\bar{U}$ may be defined as

$$\bar{U} = F - (1-G)\tan\epsilon. \tag{13·10}$$

* Equation (13·2) can be converted into the Sturm–Liouville form, to which equations variational techniques have often been applied (e.g. Courant & Hilbert 1953).

Substitution of (13·9) into (13·10) yields

$$\bar{U} = -\tan\epsilon + (M + \tan\epsilon)\,\mathrm{e}^{-z} - M\,\mathrm{e}^{-2z}, \tag{13·11}$$

where $M = \frac{1}{2}a^{-2}$. This is a function which is zero at $z = 0$, changes sign within the flow and has a limiting negative value at infinity. It is readily shown that the particular profile for which the point of inflexion is at the point of zero velocity is given by $M = 3\tan\epsilon$. Then

$$K(z) = \frac{4}{\mathrm{e}^{z} - 1}. \tag{13·12}$$

Thus the differential equation (13·2) becomes

$$w'' - \sigma^2 w + \frac{4w}{\mathrm{e}^{z} - 1} = 0. \tag{13·13}$$

This equation has an exact eigen-solution which satisfies the conditions (12·2a); it is

$$w = \mathrm{e}^{-\frac{3}{2}z} - \mathrm{e}^{-\frac{1}{2}z}, \tag{13·14}$$

with the eigenvalue, σ, equal to $\frac{3}{2}$.

The corresponding approximate value of σ can now be obtained for comparison by the variational procedure. In order to avoid the infinite range of integration in (13·4), it is well to use the transformation

$$y = 1 - \mathrm{e}^{-z}; \tag{13·15}$$

hence

$$\sigma^2 = \int_0^1 \left[\frac{K(y)\,w^2}{1-y} - (1-y)\left(\frac{\mathrm{d}w}{\mathrm{d}y}\right)^2\right]\mathrm{d}y \Big/ \int_0^1 \frac{w^2\,\mathrm{d}y}{1-y}. \tag{13·16}$$

A choice of function of the form

$$w = y(1-y)^B \tag{13·17}$$

leads, as one would expect, to the exact solution (13·14); that is, the extremal σ^2 lies at $B = \frac{3}{2}$ and is $\sigma^2 = \frac{9}{4}$. However, this cannot be said to be a fair test of the method. If the solution (13·14) were unknown, one would be inclined to choose

$$w = y(1-y)\,(1+By), \tag{13·18}$$

which satisfies (12·2a) and contains one arbitrary constant.

Substituting (13·12) and (13·18) into (13·16) and integrating, we obtain

$$\sigma^2 = \frac{10 + 10B + 2B^2}{5 + 6B + 2B^2}. \tag{13·19}$$

This has a maximum at $B = \frac{1}{4}(-5+\sqrt{5})$, which yields $\sigma^2 = \sqrt{5}$. There is also a minimum which has a negative σ^2, and therefore no physical significance. Thus, we obtain the eigenvalue

$$\sigma = \sqrt[4]{5} \sim 1{\cdot}495.$$

This is in error by $\frac{1}{3}\%$ compared with the exact value of 1·5.

For cases such as the rotating disk without suction, for which $K(y)$ is not known analytically, $K(y)$ can be approximated by a suitable function and the above procedure then pursued. As the above example indicates, the method can be expected to yield very high accuracy.

It must be emphasized that this method is applicable only to those vibrations of § 12 for which the w solutions are everywhere real; that is, case (iii) is excluded.

14. Application of the theory to the case of the rotating disk

In part I of this paper, experiments on the flow on a rotating disk are described which show that between two critical radii vortices occur which are stationary relative to the moving surface. Photographs show that the vortex axes are in the form of spirals whose radius vector decreases in the direction of rotation. Subject to the postulate that the disturbance which appears shall be fixed relative to the surface, the theory can be used to give a qualitative explanation of the phenomenon as follows. The analysis of § 12 shows that, in a local region, a neutral disturbance stationary relative to the surface is generated at infinite Reynolds number by that velocity profile which changes sign and has a point of inflexion at the point of zero velocity. This is the profile J of figure 14. Since the flow on a rotating disk is everywhere similar, and provided we neglect the effects of viscosity (i.e. finite Reynolds number) on the disturbance, the same neutral disturbance will appear everywhere. This corresponds physically to a disturbance with vortex axes in the form of equiangular (or logarithmic) spirals. Experimentally, the angle of the spiral is found to be about 103°, and the corresponding theoretical value will now be obtained for comparison.

First of all we note the form taken by the curvature coefficients for this case. Let us take polar co-ordinates r, ϕ on the disk (figure 5), the normal to a spiral making an angle ϵ with the radius. The angle ϕ is measured in the direction of rotation of the disk, the radius vector of the spiral decreasing as ϕ increases. Then the spiral is

$$r = A\,\mathrm{e}^{-\phi\tan\epsilon}, \tag{14·1}$$

where A is a parameter which defines the spiral. The orthogonal system of curves is given by

$$r = B\,\mathrm{e}^{\phi\cot\epsilon}, \tag{14·2}$$

B being another parameter.

We choose the co-ordinates α and β as

$$\left.\begin{aligned}\alpha &= a\left(\cos\epsilon\ln\frac{r}{a}+\phi\sin\epsilon\right),\\ \beta &= a\left(-\sin\epsilon\ln\frac{r}{a}+\phi\cos\epsilon\right),\end{aligned}\right\} \tag{14·3}$$

where a is a standard radial length. The normal distance from the disk is γ (figure 5).

The element $\mathrm{d}s^2 = \mathrm{d}r^2+r^2\mathrm{d}\phi^2+\mathrm{d}\gamma^2$

becomes

$$\mathrm{d}s^2 = \frac{r^2}{a^2}(\mathrm{d}\alpha^2+\mathrm{d}\beta^2)+\mathrm{d}\gamma^2, \tag{14·4}$$

and comparison with (9·5) yields $h_1 = \dfrac{r}{a}, \quad h_2 = \dfrac{r}{a}$, (14·5)

It follows from (9·16) that $m_{13} = m_{23} = 0.$ (14·6)

Noting from (14·3) that $r = a\exp\left[\dfrac{1}{a}(+\alpha\cos\epsilon-\beta\sin\epsilon)\right]$, (14·7)

we obtain

$$\left.\begin{aligned}m_{11} = m_{21} &= \frac{\delta}{r^2}a\cos\epsilon,\\ m_{12} = m_{22} &= -\frac{\delta}{r^2}a\sin\epsilon.\end{aligned}\right\} \tag{14·8}$$

Since the curvature of the logarithmic spiral is

$$\rho = \frac{r}{\cos\epsilon}, \tag{14·9}$$

we obtain from (14·8)

$$\left.\begin{aligned} m_{11} = m_{21} &= \frac{\delta}{\rho^2}\rho_a \sim \frac{\delta}{\rho_a}, \\ m_{12} = m_{22} &= \frac{\delta}{\rho^2}\rho\tan\epsilon \sim \frac{-\delta}{\rho_a}\tan\epsilon, \end{aligned}\right\} \tag{14·10}$$

where ρ_a denotes the curvature of a spiral at $r = a$. The approximate expressions are applicable if one considers a local region near $r = a$, α and β then being small.

Since ϵ is found experimentally to be of order 13°, m_{11} and m_{21} are several times larger than m_{12} and m_{22}. The curvature ρ is not very different from r, and δ is of order $\sqrt{(\nu/\omega)}$, where ω is the angular velocity of the rotating disk (Cochran 1934), so that with $V_0 = r\omega$, m_{11} and m_{21} are of order R^{-1}. This confirms the general discussion of § 10, and justifies the neglect of curvature in the inviscid theory of § 12, which will now be used to obtain the eigenvalues by means of the variational method of § 13.

The radial velocity component is $r\omega F(\zeta)$ and the tangential component $r\omega G(\zeta)$, where F and G have been tabulated by Cochran (1934) as functions of $\zeta = \gamma\sqrt{(\omega/\nu)}$. The displacement thickness (Stuart 1954) based on the tangential velocity distribution is

$$\delta_1 = 1{\cdot}271\sqrt{(\nu/\omega)},$$

so that

$$z = \frac{\gamma}{\delta_1} = \frac{\zeta}{1{\cdot}271}. \tag{14·11}$$

The velocity $\overline{U}$ is given by

$$\overline{U} = F - (1-G)\tan\epsilon. \tag{14·12}$$

For the profile (J) with the point of inflexion at the point of zero velocity, it is found numerically that $\tan\epsilon = 0{\cdot}2365$, which gives $\epsilon = 13°\,18'$.

From the power series solution (Cochran 1934) for F and G in the neighbourhood of $\zeta = 0$, we obtain

$$K(z) = -\frac{\mathrm{d}^2\overline{U}}{\mathrm{d}z^2}\Big/\overline{U} = \frac{3{\cdot}48}{z}. \tag{14·13}$$

And with $y = 1-\mathrm{e}^{-z}$, the calculated form of $\overline{U}$ can be approximated by

$$K(y) = \frac{3{\cdot}48}{y}(1-y)(1+0{\cdot}362y); \tag{14·14}$$

we assume also

$$w = y(1-y)(1+By), \tag{14·15}$$

where B is an arbitrary constant. Substituting these latter two formulae into (13·16) we have

$$\sigma^2 = \frac{0{\cdot}16533 + 0{\cdot}17400B + 0{\cdot}03665B^2}{\frac{1}{12} + \frac{1}{10}B + \frac{1}{30}B^2}. \tag{14·16}$$

This function has a maximum at $B = -0{\cdot}540$, which yields

$$\sigma = 1{\cdot}45.$$

There is also a negative, and consequently meaningless, minimum.

Thus two quantities have been determined, the angle of the spiral and the wave number, which can be compared with experiment. The theoretical angle of the spiral is 103° 18′ (corresponding to $\epsilon = 13° 18'$), which is in very good agreement with the experimental value of part I, § 7. Now from (9·16), we see that the actual wave number n is given by $h_1 \sigma/\delta_1$; but (14·5) shows that, in a local region near $r = a$, h_1 is nearly unity. Thus

$$n = \frac{1{\cdot}45}{\delta_1}, \quad \text{where} \quad \delta_1 = 1{\cdot}271\sqrt{\left(\frac{\nu}{\omega}\right)} \quad \text{(Stuart 1954)}.$$

Let us now calculate the number of spiral streaks which appear over the surface of the disk. (It is shown in § 15 that one wave-length of the disturbance corresponds to one streak in the china clay.)

Now the disturbance wave-length in α is $2\pi/n$, while from (14·3) the co-ordinate α is

$$\alpha = a\left(\cos\epsilon \ln\frac{r}{a} + \phi \sin\epsilon\right);$$

therefore, for a constant radius, the disturbance has a wave-length in ϕ of $2\pi/na\sin\epsilon$. Thus the number of vortices is

$$na\sin\epsilon = \frac{1{\cdot}45(a)\,(0{\cdot}23)}{1{\cdot}271\sqrt{(\nu/\omega)}} = 0{\cdot}262a\sqrt{\left(\frac{\omega}{\nu}\right)}. \qquad (14{\cdot}17)$$

The quantity $a\sqrt{(\omega/\nu)}$ is a Reynolds number and, apart from the factor 1·271, is nearly $R_{\delta_1} = \omega a \delta_1/\nu$. In experiment (§ 7), R_{δ_1} is found to have the range 550 to 680, the upper value indicating transition. Thus, substituting in (14·17), we have the number of vortices as 113 to 140. Actual experimental observation yields 30 (§ 7).

This discrepancy suggests that viscosity has considerable influence on the wave number, this view being supported by the low Reynolds number (R_{δ_1}) observed in experiment; for one would not expect inviscid theory to hold in this range. But it seems that viscosity has little effect on the angle ϵ.

The closeness of the wave number σ for a rotating disk with suction ($\sigma = 1{\cdot}5$) and without suction ($\sigma = 1{\cdot}45$) suggests that the function $K(z)$ for the velocity profiles with the point of inflexion at the point of zero velocity (profile J of figure 14) should be nearly the same for the two cases; this is in fact the case (Stuart 1954).

15. The streamlines in the disturbed boundary layer

In the previous section we have obtained a theoretical wave number and have related it to the spacing of the streaks occurring in the china clay. This correlation depends upon the assumption that a single streak corresponds to one wave-length of the disturbance. To show that this is the case, it is necessary to obtain the streamline pattern in the disturbed boundary layer. Now, it was pointed out (§ 14) that the cases of the rotating disk without and with suction are numerically almost identical, when the distance from the surface is related to the displacement thickness. Consequently, because of its analytical simplicity, the exact solution (§ 13) for flow on a rotating disk with large suction will be used to illustrate the streamline pattern. Additionally, the flow pattern may be expected to be typical of perturbed three-dimensional boundary layers in general.

PHILOSOPHICAL TRANSACTIONS OF THE ROYAL SOCIETY A MATHEMATICAL, PHYSICAL & ENGINEERING SCIENCES

We refer the distances x, y, z to the displacement thickness. The velocity perturbations are $(u, v, w)\,e^{i\sigma x}$, while the main flow is $(\bar{U}, \bar{V}, 0)$, with neglect of the small component of mean velocity normal to the surface.

In this case then

$$\left.\begin{aligned}\bar{U} &= \omega r \sin\epsilon[-1+4\,e^{-z}-3\,e^{-2z}],\\ \bar{V} &= \omega r \cos\epsilon[1+(3\tan^2\epsilon-1)\,e^{-z}-3\tan^2\epsilon\,e^{-2z}],\end{aligned}\right\} \tag{15·1}$$

where ϵ is the angle between the radius and the direction of propagation of the disturbance and ωr is the local velocity of the disk surface.

Using equations (10·9), (10·10), (10·11) and (13·13) with R^{-1} terms neglected, and taking real parts, we obtain for the total flow velocities

$$u = \bar{U} + 2a(e^{-\frac{3}{2}z} - \tfrac{5}{3}e^{-\frac{5}{2}z})\sin\tfrac{3}{2}x, \tag{14·2}$$

$$v = \bar{V} + \frac{4a}{3}\frac{e^{-\frac{5}{2}z}}{\tan\epsilon(-1+3\,e^{-z})}[(3\tan^2\epsilon-1)-6\tan^2\epsilon.e^{-z}]\sin\tfrac{3}{2}x, \tag{15·3}$$

$$w = 2a(e^{-\frac{3}{2}z} - e^{-\frac{5}{2}z})\cos\tfrac{3}{2}x, \tag{15·4}$$

where $2a$ is an arbitrary amplitude constant. The perturbation velocities u and v are non-zero at the wall ($z=0$), but would be reduced to rest by viscosity in practice; similarly, the singularity in V at $z=\ln 3$ would be eliminated by viscous action.

Now let us consider the projection of the streamline pattern on to the x, z plane; from (15·1), (15·2) and (15·4) it follows that these projected streamlines are given by

$$\tfrac{2}{3}b\sin\tfrac{3}{2}x = \frac{d-z-4\,e^{-z}+\frac{3}{2}e^{-2z}}{e^{-\frac{3}{2}z}-e^{-\frac{5}{2}z}}, \tag{15·5}$$

where $b = 2a/\omega r\sin\epsilon$, and d is a constant which specifies the particular streamline. If we take $b = 1$, then the maximum modulus of w is about 0·185 of the maximum modulus of $\bar{U}$. The streamlines projected on to the x, z plane are shown in figure 16 for the case $b = 1$. Not all the streamlines have been calculated accurately, for the main thing is to determine the vortex centres, C, C', F, etc., the streamline crossing points E, E', etc., and the boundary streamlines ADB, $A'D'B'$. Also, it is known that the general stream $\bar{U}$ for large z is in the negative x direction. Since the flow is rotational, the streamlines at E, E' do not cut at right angles, and in fact the angle of intersection is about 37·5°. The points A, A', B, B', C, C', E, E', F, etc., are stagnation points.

It can be seen from figure 16 that the vortices away from the wall all rotate in the same direction, while the vortices near to the wall are staggered relative to the outer ones and all rotate in the opposite direction.

The shear stress is obtained by differentiation of (15·1), (15·2) and (15·3). This yields

$$\frac{1}{\omega r\sin\epsilon}\left(\frac{\partial u}{\partial z}\right)_0 = 2+\tfrac{8}{3}b\sin\tfrac{3}{2}x, \tag{15·6}$$

$$\frac{1}{\omega r\cos\epsilon}\left(\frac{\partial v}{\partial z}\right)_0 = (1+3\tan^2\epsilon)+b(\tfrac{1}{3}+3\tan^2\epsilon)\sin\tfrac{3}{2}x, \tag{15·7}$$

the suffix zero denoting the wall.

Since b is positive, each of these quantities takes its maximum modulus at $x = \frac{1}{3}\pi, \frac{5}{3}\pi$, etc., that is, at the points G, G', etc., of figure 16. The resultant shear stress at the surface is

proportional to the resultant of the quantities (15·6) and (15·7). It seems probable that, for streaks to appear, the disturbance must have been amplified sufficiently to cause a large peak in the shear stress at $\frac{1}{3}\pi$, $\frac{5}{3}\pi$. This does, in fact, occur when $b = 1$, for the ratio of shear stress at $x = \frac{1}{3}\pi$ to that at $x = \pi$ is $\sqrt{(53 + 36\tan^2\epsilon + 81\tan^4\epsilon)}/\sqrt{2}$. For the rotating disk without suction, for which the velocity distribution (1) is a good approximation, $\tan\epsilon$ is about $\frac{1}{4}$, and we obtain

$$\left(\frac{\partial v}{\partial z}\right)_{0,\max.} \Big/ \left(\frac{\partial u}{\partial z}\right)_{0,\max.} = 1{\cdot}49,$$

and the two components of shear stress are of similar magnitude. The direction of the shear is at about 35° to the y direction. It follows that streaks occur on the lines defined by $z = 0$; $x = \frac{1}{3}\pi, \frac{5}{3}\pi$, etc., that is, on a series of lines in the y direction under the wall vortices. There is thus one streak per wave-length.

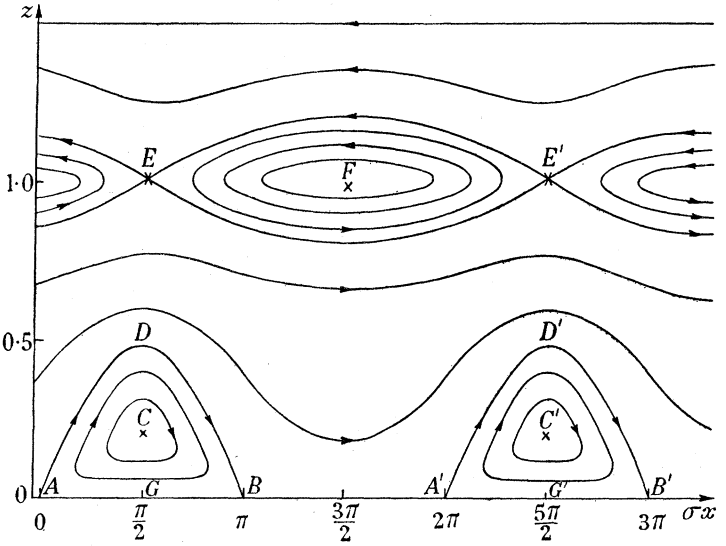

FIGURE 16. Vortices generated by three-dimensional instability.

The effect of viscosity on the flow pattern is to increase the wave-length of the disturbance because of dissipation, and to reduce the perturbation velocity at the wall to zero. This will cause some modification of the flow pattern near to the wall, but since the viscous perturbation velocity rises with distance from the wall more rapidly than the main flow velocity, a system of vortices as discussed here may be expected in the viscous case also.

(*a*) *The Görtler case*

Having seen how the china-clay streaks are produced in the case of the unstable flow on a rotating disk, we shall now discuss the mechanism producing similar streaks in the case of flow over a concave wall (as observed by Gregory & Walker 1950).

The equations relevant to this type of instability are given by equations (10·7), and can be written in the form

$$\left(\frac{\partial^2}{\partial z^2} - \sigma^2\right)^2 w_1 = -2\sigma^2 \frac{\delta}{a} R^2 v_1 \overline{V},$$

$$\left(\frac{\partial^2}{\partial z^2} - \sigma^2\right) v_1 = w_1 \frac{\partial \overline{V}}{\partial z},$$

$$u_1 = \frac{\mathrm{i}}{\sigma}\frac{\partial w_1}{\partial z},$$

where the perturbation velocities are u_1, Rv_1, and w_1, R is the Reynolds number and σ is the wave number for a neutral disturbance.

The total velocity components are

$$u = -\frac{V_0 a}{\sigma}\frac{\partial w_1}{\partial z}\sin \sigma x,$$

$$v = V_0[\overline{V} + aRv_1(z)\cos \sigma x],$$

$$w = V_0 a w_1(z)\cos \sigma x.$$

The occurrence of the Reynolds number factor, R, in the perturbation velocity in the stream direction means that the shear stress in that direction is very much larger than that in the transverse direction. Thus we need consider only the v component of shear stress. If $(\partial \overline{V}/\partial z)_0$ and $aR(\partial v_1/\partial z)_0$ are of the same sign and order of magnitude, streaks occur at $\sigma x = 0, 2\pi$, etc. But if they are of opposite sign but same order of magnitude the streaks occur at $\sigma x = \pi, 3\pi$, etc. A simple analysis shows the latter case to hold, in agreement with physical ideas. One streak occurs per wave-length, and at a position between the pair of vortices where the fluid is moving towards the surface (at K and K' of figure 17).

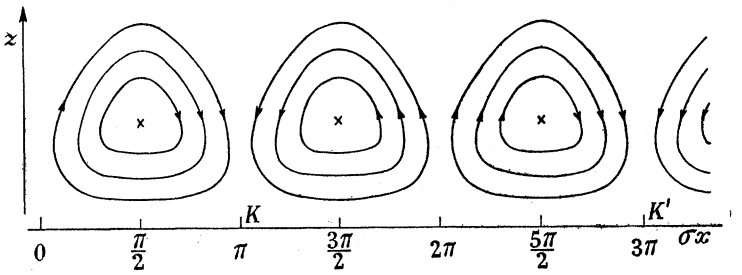

FIGURE 17. Görtler vortices.

(b) Comparison of rotating disk and Görtler cases

(i) The vortex pattern is determined by the combination of main flow and perturbation flow.

(ii) In a three-dimensional boundary layer exhibiting inflexional instability, the steady vortex pattern consists of two rows of vortices. One row is close to the wall, while the other is farther away from the wall.

(iii) In the case of Görtler instability in a boundary layer, streaks in the china clay appear *between* alternate pairs of vortices, whereas the streaks are *underneath* the wall vortices in the three-dimensional case.

(iv) The shear which produces streaks in Görtler's case is primarily streamwise, whereas in the three-dimensional case, streamwise and transverse shear components contribute in similar proportions.

Part III. DISCUSSION

By N. GREGORY and J. T. STUART

16. Correlation between theoretical and experimental work

The china-clay technique, as illustrated by the photographs of a swept-wing surface (figure 3) and of a rotating-disk surface (figure 4), shows that along certain curves on the surface the shear stress is very much higher than at other regions of the surface. By analogy with similar experimental evidence in the case of Görtler vortices (Gregory & Walker 1950), it is inferred that the curves of high shear stress denote the axial directions of a boundary-layer vortex system which is fixed relative to the surface. On the other hand, the frequency analysis of the rotating-disk boundary layer indicates, within the instability region, a spread of amplitude about a sharp peak. It is known that this spread is not due to the apparatus. Consequently, it can be inferred that there is a real physical spread about the peak frequency. Some of the frequencies within this region of spread in amplitude correspond to fixed vortices of different spacing, while others correspond to waves in motion relative to the surface. Naturally, the china-clay technique indicates only these disturbances which are fixed relative to the surface. The slight lack of uniformity in spacing of the vortices on the disk (figure 4) may be attributed to the superposition of several fixed-vortex patterns of slightly different wave-lengths upon a dominant pattern.

Now it has been demonstrated theoretically that many different modes of instability are possible in a three-dimensional boundary layer. Most of the disturbances consist of progressive wave patterns, but at any particular station in the flow there is certainly one mode of disturbance which is stationary relative to the surface. If such a disturbance appears everywhere, the result is a pattern of fixed disturbance vortices. Indeed, we may relate this theoretical vortex pattern to the pattern, described above, which is shown up by the china-clay technique. The other components of the physical wave packet may be neighbouring neutral and amplified waves of either zero or finite wave velocity, and with the vortex axes on curves slightly differing from one another. These neighbouring waves may combine to give the frequency spectrum and the slight irregularity in the spacing of vortices observed experimentally.

As one follows the path of a vortex in the direction of increasing Reynolds number, it is thought that the disturbances increase in magnitude until they are sufficiently large in magnitude to produce transition to turbulence. But at any particular station on the surface the amplitude of the disturbance there has a fixed value, and neither amplifies nor decays. (It may be noted that the cases of a boundary layer on a swept wing and on a rotating disk are in one sense qualitatively different—in the former case the increase of Reynolds number takes place most rapidly in the main-flow direction, whereas in the latter case it takes place most rapidly in a direction at right angles to the main-flow direction. Since the steady-vortex axes lie at a fairly small angle to the main-flow direction, this means that in the rotating-disk case the vortices may cover a greater distance from the point of instability to transition than in the swept-wing case. Although, if the vortices pass out of the unstable region on the wing before transition occurs, they may persist for some distance before becoming completely damped out, or until transition intervenes.)

PHILOSOPHICAL TRANSACTIONS OF THE ROYAL SOCIETY A MATHEMATICAL, PHYSICAL & ENGINEERING SCIENCES

Now in the theoretical calculation of the eigenvalues of the problem, the case worked out in detail has been that of a disturbance of zero wave velocity on a rotating disk. The angle of the spiral—about 103°—is in extremely good agreement with experiment,* while the wave number, which gives the spacing of the vortices, is approximately four times too large. Thus it appears that the inertial forces producing the inflexional instability determine the *directional* mode, this being little affected by viscous damping, while the wave number drops with Reynolds number because of the dominance of viscous damping at larger wave numbers. In order to calculate the actual wave number corresponding to a finite Reynolds number, it is necessary to perform a more elaborate calculation, which would yield also a critical Reynolds number of instability and modify slightly the precise form of the spiral. There are five parameters involved, the Reynolds number (R), the wave number (σ), the complex wave velocity (c_r) and amplification factor (c_i), and the directional parameter (ϵ); the quantity ϵ is the additional parameter necessitated by three-dimensionality.

A fundamental problem which has not been solved in this paper is the reason why a disturbance which is stationary relative to the surface appears to be a dominant one (or one of the dominant ones) over a considerable area of instability. The acoustic spectrum analysis of the boundary layer shows up a sharp peak at a certain frequency, but the analysis is not accurate enough to show conclusively that the actual peak corresponds to a fixed vortex. However, the frequency change between neighbouring fixed vortices in the frequency scale is only 30 c/s, which means that one or more fixed vortices are associated with large amplitude disturbances. Consequently, in the wave packet there are components of large amplitude which are stationary relative to the surface, and which may produce streaks in the china clay. It may be assumed that the components of the disturbance with large amplitudes are associated with the most unstable disturbances (of greatest amplification) of linearized instability theory.† Thus the mathematical problem consists of finding the eigenvalues of the most highly amplified disturbance components, and of showing that one or more components with zero wave velocity are included within this highly amplified zone of the spectrum. It may be, however, that the fixed-vortex components (of the frequency spectrum) are more highly favoured for amplification by factors such as surface roughness, which are outside the scope of linearized theory of instability.

Earlier in this section it has been mentioned that a disturbance wave packet at a given point (or small region of space) is neutral. The reason for this appears to be that the amplified disturbances generated according to instability theory are convected as they amplify, with the consequent result that an amplified disturbance which is convected out of the small region is replaced by another (less amplified) disturbance which is convected into the region. More concisely, a disturbance which, according to linearized theory of instability, is amplified exponentially with time, in an actual boundary layer of varying Reynolds number is amplified exponentially with distance. The rotating-disk oscillations shown by Smith (1947) illustrate this, as well as the results of this paper. Similar experimental evidence for a two-dimensional boundary layer was given by Schubauer & Skramstad (1943).

* This means an angle of about 13° to the direction of rotation, compared with typical angle of 2 or 3° for the inclination of vortices to streamlines on a swept wing. The reason for this difference is the much smaller magnitude of the secondary (N) profile in the swept-wing case than in the rotating-disk case.

† One of us (J.T.S.) is indebted to Dr G. K. Batchelor for an elucidative discussion on this point.

PHILOSOPHICAL TRANSACTIONS OF THE ROYAL SOCIETY A MATHEMATICAL, PHYSICAL & ENGINEERING SCIENCES

The way in which the streaks in the china clay are associated with a double-row vortex system has been shown theoretically, but it has not yet been found possible to illustrate this experimentally.

17. Application of three-dimensional stability theory to other situations

It was noticed by Luthander & Rydberg (1935) that the critical speed for a sphere which is rotating uniformly about an axis parallel to the stream at first rises with the angular velocity, but ultimately drops. It was suggested by Schlichting (1953) that the initial rise in the critical speed was caused by a shift of the laminar separation towards the equator from the value 81° at zero rotation. He also suggested that at higher rotational speeds, the rotation of the sphere might destabilize the boundary layer, thus causing transition of the

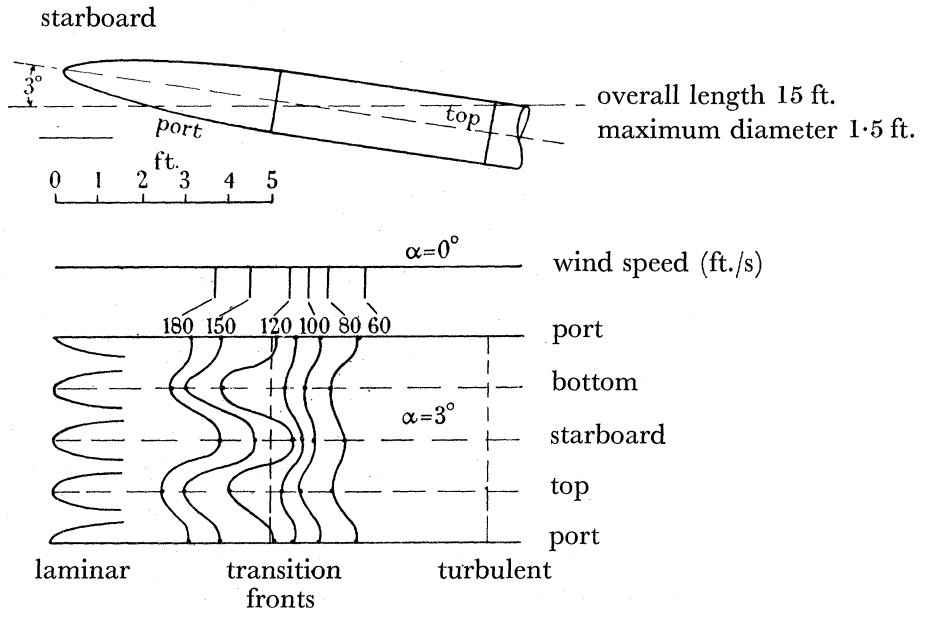

Figure 18. Development of surface of body of revolution showing affect of yaw on transition.

boundary layer to occur for a lower speed of the main stream. The work described in this paper confirms this view, since the inflexional instability of a three-dimensional boundary layer (which is generated by rotation of the sphere) is very much more powerful than the viscous instability of an axisymmetric boundary layer.

Again, the boundary layer present on a yawed body of revolution has varying degrees of three-dimensionality (given by the magnitude of the secondary profile N of figure 14), which means that the critical Reynolds number varies considerably, as has been observed in transition experiments at the National Physical Laboratory (figure 18). On the port side, where the flow is retarded and quasi-two-dimensional, the transition point is slightly further forward than at zero yaw. On the starboard, in the accelerated and quasi-two-dimensional region, it is slightly further back. But it is generally much further forward at the top and bottom, because of the much more unstable (three-dimensional) boundary layer which is present there.

The experiments described by Gregory & Walker (1950) on the flow past excrescences show that a horseshoe vortex is developed around an excrescence in a boundary layer.

Under certain critical conditions other vortices are developed further downstream with axes in the stream direction, these other vortices having stations outboard of the horse shoe vortex. These extra (steady) vortices may be formed by an instability of a three-dimensional flow developed by the original horseshoe vortex, a three-dimensionality of the flow becoming sufficient only at some distance downstream from the excrescence. The phenomenon is illustrated by figure 19. The authors are indebted to Sir Geoffrey Taylor, F.R.S., for this suggested explanation of the phenomenon.

Appendix to § 10. *Effect of* $m_{\nu\mu}$ *and* δ'_ν *terms on stability*

It is customary in cases of two-dimensional stability to separate solutions of the Orr–Sommerfeld equation into (1) inviscid and (2) viscous integrals. For (1), all terms in R^{-1} are neglected, and for (2) a certain transformation of independent variable is made. Again for the present case, if terms of order R^{-1} are neglected the $m_{\nu\mu}$ and δ'_ν terms have no effect on the inviscid integrals, except perhaps in the regions around $\overline{U} = c$ (see § 12). Let us now derive the equations for the viscous integrals and for the modifications to the inviscid integrals near $\overline{U} = c$ (that is, in the region of the singularities mentioned in § 12).

We shall now develop solutions in powers of ϵ_1 near one critical point (z_1) and ϵ_2 near to the other (z_2), where the parameters ϵ_1 and ϵ_2 are given by

$$\epsilon_1 = (\sigma R \overline{U}'_1)^{-\frac{1}{3}} \quad \text{and} \quad \epsilon_2 = (\sigma R \overline{U}'_2)^{-\frac{1}{3}}, \tag{A 1}$$

where $\overline{U}'_1$ and $\overline{U}'_2$ denote gradients of $\overline{U}$ at z_1 and z_2 respectively.

Considering just one critical point, we write

$$\left.\begin{aligned} z_1 &= \epsilon_1 \eta_1, \\ \overline{U} - c &= \overline{U}'_1 \epsilon_1 \eta_1 + \tfrac{1}{2} \overline{U}''_1 \epsilon_1^2 \eta_1^2 + \ldots, \\ \overline{V} &= \overline{V}_1 + \epsilon_1 \eta_1 \overline{V}'_1 + \ldots, \\ \overline{W} &= \overline{W}_1 + \epsilon_1 \eta_1 \overline{W}'_1 + \ldots, \\ w &= w_0 + \epsilon_1 w_1 + \epsilon_1^2 w_2 + \ldots, \\ v &= v_0 + \epsilon_1 v_1 + \epsilon_1^2 v_2 + \ldots. \end{aligned}\right\} \tag{A 2}$$

Substitution of (A 2) into (9·17) and retention of only terms of order $1/\epsilon_1$ and $(\epsilon_1)^0$, we have

$$\left.\begin{aligned} \eta_1 w''_0 + \mathrm{i} w_0^{\mathrm{iv}} &= 0, \\ \eta_1 w''_1 + \mathrm{i} w_1^{\mathrm{iv}} &= \frac{\overline{U}''_1}{\overline{U}'_1} w_0 - \frac{1}{2} \frac{\overline{U}''_1}{\overline{U}'_1} \eta_1^2 w''_0 + \mathrm{i} A \overline{W}_1 w''_0, \end{aligned}\right\} \tag{A 3}$$

where dashes in w_0 and w_1 denote differentiation with respect to η_1, and $\delta'_3 = A/R$. It is seen from the definition in (9·16), and known from ordinary boundary-layer theory, that δ'_3 is proportional to R^{-1}.

The first equation (A 3) is identical with that for the viscous integrals in two-dimensional boundary-layer theory. It can be inferred then, that provided one neglects terms in ϵ_1 in (A 2), the viscous integrals are independent of the $m_{\nu\mu}$ and δ'_ν terms. In the present case, of course, it is necessary to obtain expansions for the viscous integrals about each critical point to link them together; but this need not trouble us here.

The modification to the inviscid integrals near to the first critical point z_1 is obtained by substitution of $w_0 = 1$ into the second equation (A 3). It is then necessary to obtain a solution which has logarithmic tendencies for large η_1 (that is, to fit in with the solutions given in § 12). Thus the $m_{\nu\mu}$ and δ'_ν have no effect here either.

It can be concluded that the curvature terms have little influence on stability in a local region of flow, provided that the above type of analysis is valid.

The work described above was carried out in the Aerodynamics Division of the National Physical Laboratory, and this paper was submitted for publication on the recommendation of the Aeronautical Research Council and by permission of the Director of the Laboratory.

References

Anscombe, A. & Illingworth, L. N. *Rep. Memor. Aero. Res. Coun., Lond.*, (in the press).
Cochran, W. G. 1934 *Proc. Camb. Phil. Soc.* **30**, 365.
Courant, R. & Hilbert, D. 1953 *Methods of mathematical physics*, **1**. New York: Interscience.
Fage, A. 1938 *Proc. Roy. Soc.* A, **165**, 501.
Foote, J. R. & Lin, C. C. 1950 *Quart. Appl. Math.* **8**, 265.
Frank, P. & Mises, R. von 1930 *Die Differential- und Integralgleichungen der Mechanik und Physik*, **1**. Braunschweig: Verlag Vieweg.
Goldstein, S. 1935 *Proc. Camb. Phil. Soc.* **31**, 232.
Goldstein, S. 1937 *Proc. Camb. Phil. Soc.* **33**, 41.
Goldstein, S. 1938 *Modern developments in fluid dynamics*. Oxford: Clarendon Press.
Görtler, H. 1940*a* *Nachr. Ges. Wiss. Göttingen*, (2), no. 1.
Görtler, H. 1940*b* *Z. angew. Math. Mech.* **20**, 138.
Gray, W. E. *Rep. Memor. Aero. Res. Coun., Lond.*, (to be published).
Gregory, N. & Walker, W. S. 1946 *Rep. Memor. Aero. Res. Coun., Lond.*, no. 2287.
Gregory, N. & Walker, W. S. 1950 *Rep. Memor. Aero. Res. Coun., Lond.*, no. 2779.
Heisenberg, W. 1924 *Ann. Phys., Lpz.*, (4), **74**, 577.
Hollingdale, S. H. 1940 *Phil. Mag.* (7), **29**, 209.
Howarth, L. 1951 *Phil. Mag.* (7), **42**, 239.
Jones, R. T. 1947 *N.A.C.A. Rep.* no. 884.
Kármán, T. von 1921 *Z. angew. Math. Mech.* **1**, 235.
Kármán, T. von 1934 *Proc. Fourth Int. Congr. Appl. Mech.* p. 60. Cambridge: University Press.
Kuethe, A. M. 1950 *Proc. First Mid-West Conf. Fluid Dynamics*. Ann Arbor, Mich.: J. W. Edwards.
Liepmann, H. W. 1945 *N.A.C.A. Wartime Rep.* no. W.8.
Lin, C. C. 1945 *Quart. Appl. Math.* **3**, 117, 218, 277.
Luthander, S. & Rydberg, A. 1935 *Phys. Z.* **36**, 552.
Owen, P. R. & Randall, D. G. (to be published).
Pai, S. I. 1951 *J. Aero. Sci.* **18**, 731.
Pretsch, J. 1941 *Jb. dtsch. Luftfahrtf.* **1**, 58.
Rayleigh, Lord 1880 *Scientific papers*, **1**, 474; **3**, 17; **4**, 203; **6**, 197.
Reynolds, O. 1883 *Collected papers*, **2**, 51.
Richards, E. J., Walker, W. S. & Taylor, C. R. 1945 *Rep. Memor. Aero. Res. Coun., Lond.*, no. 2149.
Savic, P. 1941 *Phil. Mag.* (7), **32**, 245.
Schlichting, H. 1933 *Nachr. Ges. Wiss. Göttingen, Math. Phys. Kl.*, p. 182.
Schlichting, H. 1935 *Nachr. Ges. Wiss. Göttingen, Math. Phys. Kl.*, p. 47.
Schlichting, H. 1951 *Grenzschicht-Theorie*. Karlsruhe: Verlag Braun.
Schlichting, H. 1953 *Ingen-Arch.* **21**, 227.

PHILOSOPHICAL TRANSACTIONS OF THE ROYAL SOCIETY A MATHEMATICAL, PHYSICAL & ENGINEERING SCIENCES

Schubauer, G. B. & Skramstad, H. K. 1943 *J. Res. Nat. Bur. Stand.* **38**, 25 (published 1947), *N.A.C.A. Rep.* no. 909 (published 1950).
Sears, W. R. 1948 *J. Aero. Sci.* **15**, 49.
Shibuya, I. 1951 *Rep. Inst. High-Speed Mech.*, Tôhoku Univ., **1**, 27.
Smith, N. H. 1947 *Tech. Notes Nat. Adv. Comm. Aero., Wash.*, no. 1227.
Squire, H. B. 1933 *Proc. Roy. Soc.* A, **142**, 621.
Stuart, J. T. 1954 *Quart. J. Mech.* **7**, 446.
Taylor, G. I. 1915 *Phil. Trans.* A, **215**, 23.
Taylor, G. I. 1923 *Phil. Trans.* A, **223**, 289.
Theodorsen, T. & Regier, A. 1947 *N.A.C.A. Rep.* no. 793.
Tietjens, O. G. 1925 *Z. angew. Math. Mech.* **5**, 200.
Tollmien, W. 1929 *Nachr. Ges. Wiss. Göttingen, Math. Phys. Kl.*, p. 21.
Tollmien, W. 1935 *Nachr. Ges. Wiss. Göttingen, Math. Phys. Kl.*, p. 79.

PHILOSOPHICAL TRANSACTIONS OF THE ROYAL SOCIETY A MATHEMATICAL, PHYSICAL & ENGINEERING SCIENCES

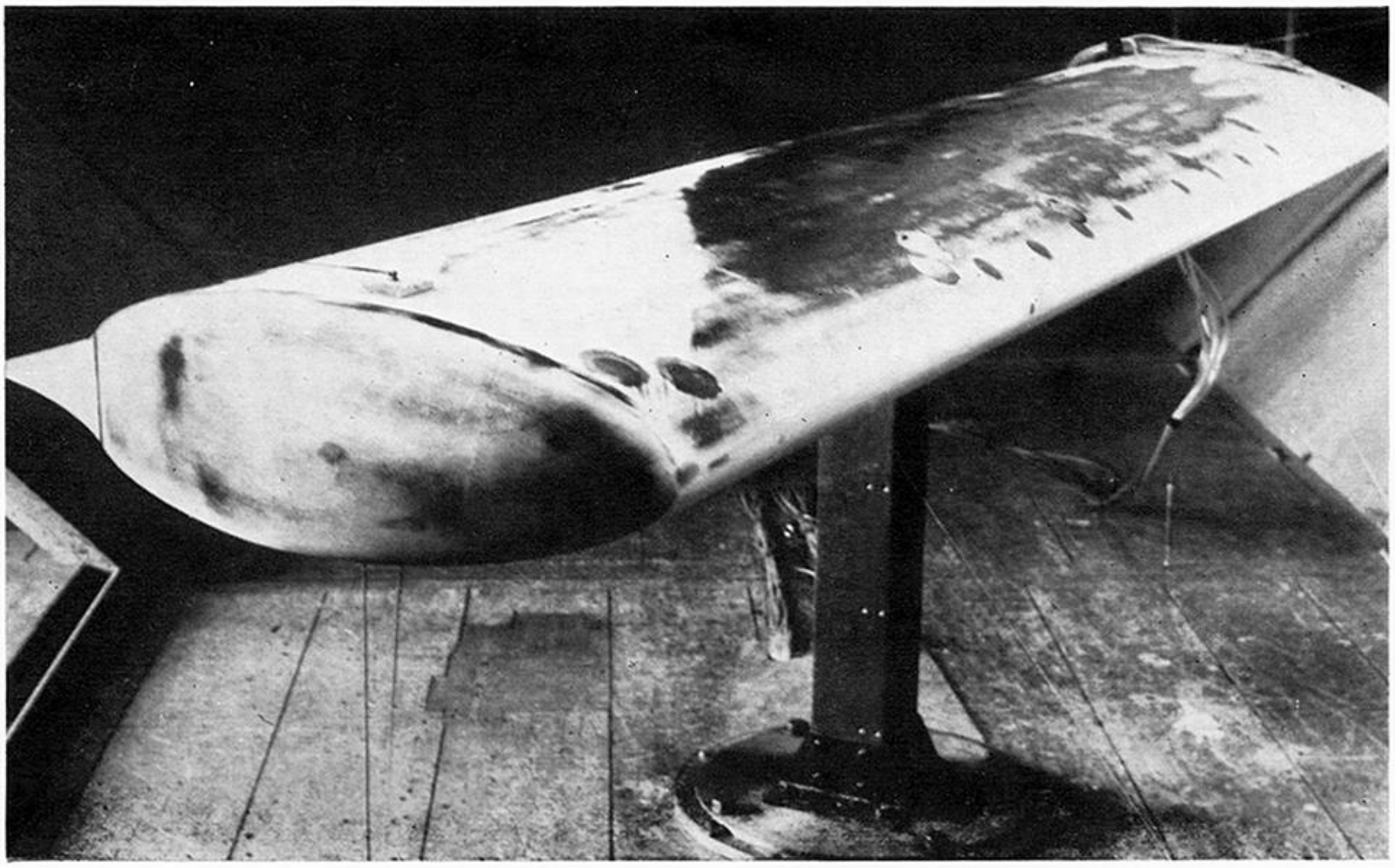

FIGURE 1. General view of arrangement of 30 % Griffith aerofoil in tunnel. Sweep angle 60°. Transition at 100 ft./s.

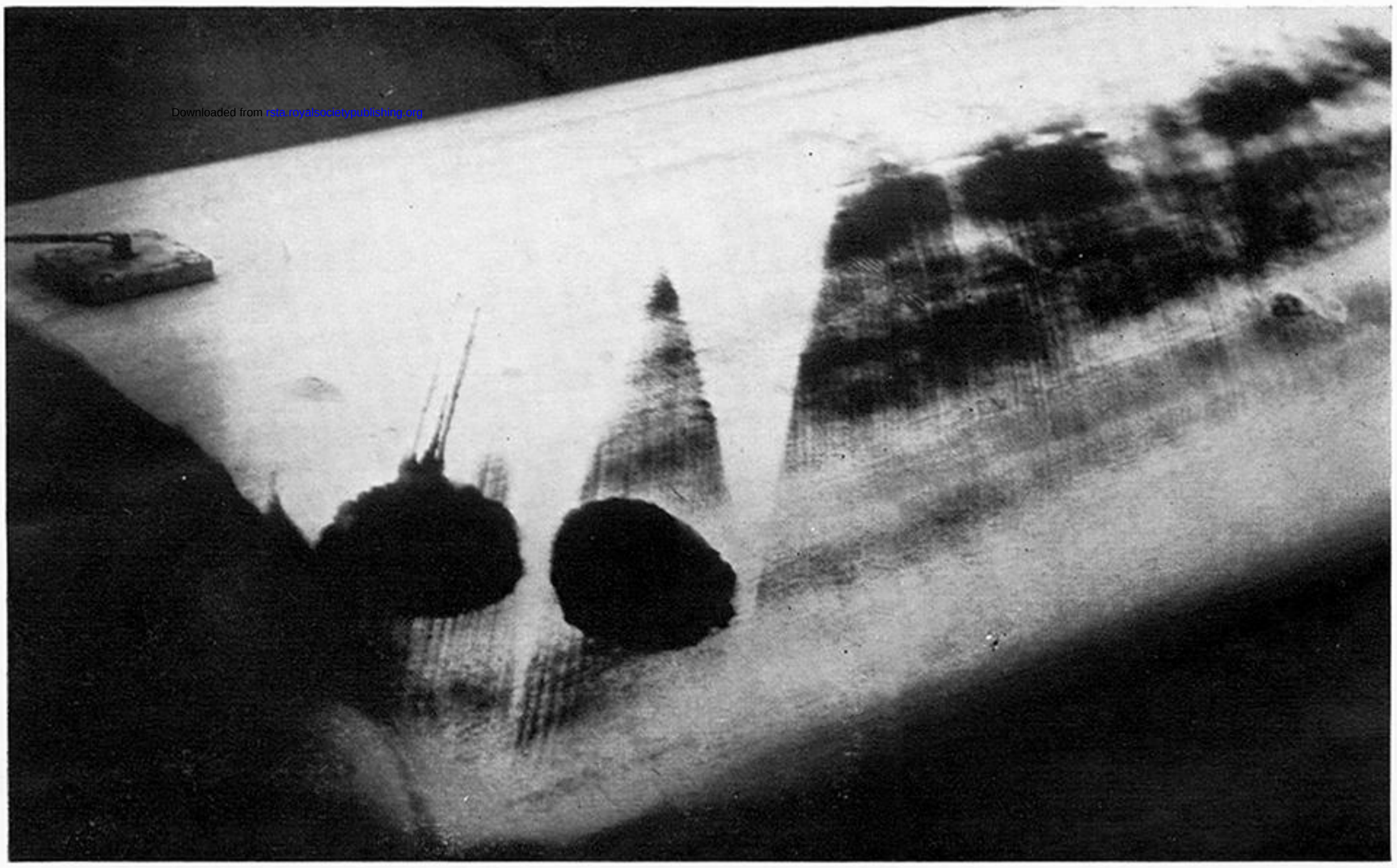

FIGURE 3. China-clay record of vortex traces persisting to transition at 0·4 chord on 30 % Griffith aerofoil. Sweep angle 45°. Wind speed 180 ft./s.

(*Facing p.* 162)

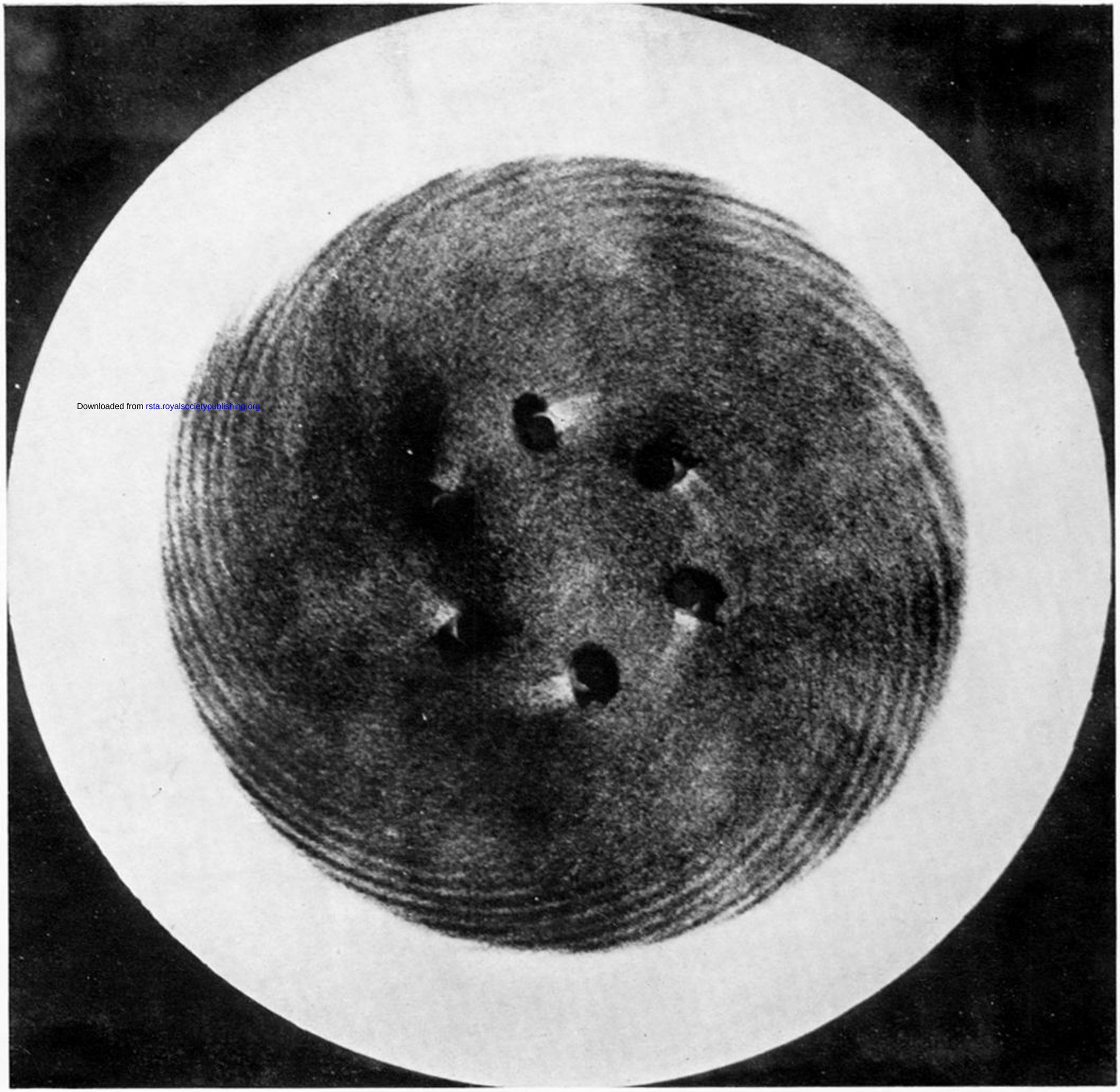

FIGURE 4. China-clay record of instability and transition on a rotating disk. Direction of rotation of disk: anti-clockwise. Rotational speed 3200 rev/min. Radius of disk 6 in. Radius at start of instability 3·5 in. R_r ($\equiv r^2\omega/\nu$) = 182000. Radius at transition 4·35 in. $R_r = 282000$.

PHILOSOPHICAL TRANSACTIONS OF THE ROYAL SOCIETY A MATHEMATICAL, PHYSICAL & ENGINEERING SCIENCES

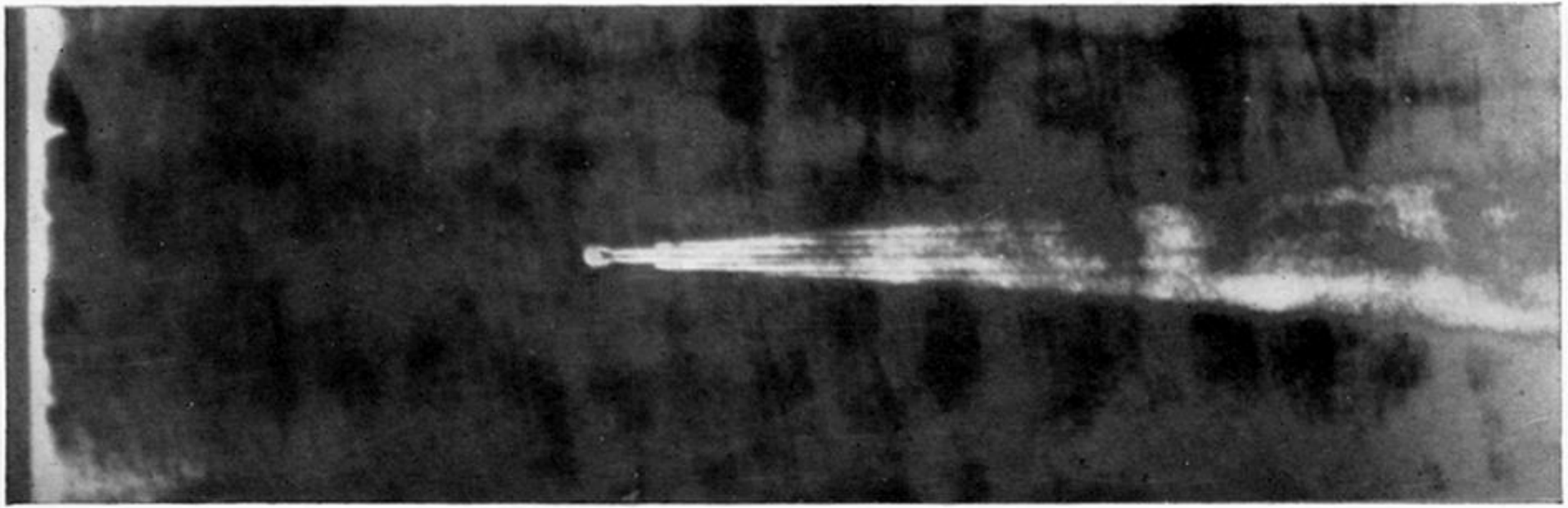

IGURE 19. China-clay record of vortex structure of a turbulent wake on a flat plate. Cylindrical excrescence, height 0·04 in., diameter 0·2 in. 0·75 ft. from leading edge; wind speed 40 ft./s.